Front. Med. 2025, 19(1): 149−169
https://doi.org/10.1007/s11684-024-1089-z

RESEARCH ARTICLE

Decreased neurotensin induces ovulatory dysfunction via the NTSR1/ERK/EGR1 axis in polycystic ovary syndrome

Dongshuang Wang[1,2,*], Meiling Zhang[1,2,*], Wang-Sheng Wang[1,2], Weiwei Chu[1,2], Junyu Zhai[1,2], Yun Sun[1,2], Zi-Jiang Chen (✉)[1,2,3], Yanzhi Du (✉)[1,2]

[1]Center for Reproductive Medicine, Ren Ji Hospital, School of Medicine, Shanghai Jiao Tong University, Shanghai 200135, China; [2]Shanghai Key Laboratory for Assisted Reproduction and Reproductive Genetics, Shanghai 200135, China; [3]National Research Center for Assisted Reproductive Technology and Reproductive Genetics, The Key Laboratory for Reproductive Endocrinology of Ministry of Education, Shandong Provincial Key Laboratory of Reproductive Medicine, Center for Reproductive Medicine, Shandong Provincial Hospital, Shandong University, Jinan 250012, China

Abstract **Polycystic ovary syndrome (PCOS) is the predominant cause of subfertility in reproductive-aged women; however, its pathophysiology remains unknown. Neurotensin (NTS) is a member of the gut–brain peptide family and is involved in ovulation; its relationship with PCOS is unclear. Here, we found that NTS expression in ovarian granulosa cells and follicular fluids was markedly decreased in patients with PCOS. In the *in vitro* culture of cumulus–oocyte complexes, the neurotensin receptor 1 (NTSR1) antagonist SR48692 blocked cumulus expansion and oocyte meiotic maturation by inhibiting metabolic cooperation and damaging the mitochondrial structure in oocytes and surrounding cumulus cells. Furthermore, the ERK1/2-early growth response 1 pathway was found to be a key downstream mediator of NTS/NTSR1 in the ovulatory process. Animal studies showed that *in vivo* injection of SR48692 in mice reduced ovulation efficiency and contributed to irregular estrus cycles and polycystic ovary morphology. By contrast, NTS partially ameliorated the ovarian abnormalities in mice with dehydroepiandrosterone-induced PCOS. Our findings highlighted the critical role of NTS reduction and consequent abnormal NTSR1 signaling in the ovulatory dysfunction of PCOS, suggesting a potential strategy for PCOS treatment.**

Keywords neurotensin; neurotensin receptor 1; early growth response 1; polycystic ovary syndrome; ovulatory disfunction

Introduction

Polycystic ovary syndrome (PCOS), a complicated genetic condition, is a heterogeneous endocrine disorder indicated by clinical and/or biochemical hyperandrogenism, polycystic ovarian morphology, and oligo-anovulatory ovarian dysfunction. Despite its high prevalence (5%–20%) [1], the etiology of PCOS remains ambiguous. This illness accounts for 70% of females with anovulation infertility [2], which is caused by the cessation of follicular maturity and the aggregation of small antral follicles at the ovary's periphery. Females with PCOS are highly susceptible to abnormal intrafollicular microenvironments and poor oocyte developmental capacity [3]. Recent single-cell RNA sequencing has uncovered differentially expressed genes (DEGs) in PCOS oocytes that are predominantly associated with meiosis, hormone receptor signaling, and DNA repair, reflecting the inferior quality of oocytes in patients with PCOS [4]. Despite intensive research, illustrating the molecular mechanisms involved in anovulation in PCOS remains a challenge.

Neurotensin (NTS), a member of the gut–brain peptide family, is predominantly distributed in the digestive tract and neurological system of mammals [5]. This endogenous 13-amino-acid peptide is primarily involved in thermoregulation, food and water intake, pain modulation, and certain neurological disorders [6–9]. Most of the biological effects of NTS are mediated by its high selectivity to neurotensin receptor 1 (NTSR1), a member of the G protein-coupled receptor family [10]. NTS binding to NTSR1 triggers the activation of four major pathways: (1) Rho GTPases, (2) PKC/RAF-1/

Received February 9, 2024; accepted May 19, 2024

Correspondence: Zi-Jiang Chen, chenzijiang@hotmail.com;
Yanzhi Du, duyz@sjtu.edu.cn

*These two authors contributed equally to this work.

MAPK-ERK1/2, (3) intracellular Ca^{2+} release, and (4) PI3K/AKT [11]. Several studies have underlined the importance of NTSR1 in multiple pathologic conditions, such as schizophrenia and solid cancers [11–13]. After the stimulation of ovulatory gonadotropin, NTS expression in ovarian granulosa cells (GCs) rises rapidly, highlighting its crucial role as a candidate paracrine mediator of ovulation [14]. Despite the extensive studies, the possible biological actions of NTS/NTSR1 and the downstream signaling pathways in the development of anovulation in patients with PCOS remain unknown.

Ovulation is essential for the propagation and survival of mammals. This complicated process includes oocyte maturation, cumulus cell (CC) expansion, and follicular rupture, all of which are initiated by the surge of luteinizing hormone (LH) [15]. The metabolic interaction between oocytes and CCs plays a crucial role in ovulation [16–18]. Moreover, oocytes produce energy mainly through mitochondrial oxidative phosphorylation [19]. In addition to participating in energy equilibrium, mitochondria are the pivotal hubs that regulate redox and metabolism balance. Mitochondrial dysfunction reduces adenosine triphosphate (ATP) and increases reactive oxygen species (ROS), contributing to poor oocyte development [20].

Extracellular signal-regulated kinase 1/2 (ERK1/2), one component of mitogen-activated protein kinase (MAPK) pathways, is important in the LH-induced regulation of ovulation and luteinization-associated processes *in vivo* [15]. The *Erk1/2*$^{gc-/-}$ mouse model demonstrated that ERK1/2 impairment in GCs results in ovulation failure and eventual infertility [21]. Early growth response 1 (EGR1) is a zinc-finger transcription factor originally identified in quiescent cells as an immediate-early gene activated by fetal bovine serum. It was transiently induced by several extracellular signals, including cytokines, hormones, and growth factors [22,23]. Its expression is increased in the GCs of follicles following human chorionic gonadotropin (hCG) administration [24]. *Egr1*$^{-/-}$ female mice are infertile because they are deficient of the LH β-subunit in the pituitary–gonadal axis [25], indicating that EGR1 might participate in ovulatory function control. ERK1/2 is an upstream activator of EGR1 [26,27]. Given its ability to trigger the ERK1/2 pathway, we suspected that NTS/NTSR1 may be involved in ovulation through the activation of the ERK1/2-EGR1 signaling pathway.

In this study, we found that NTS was markedly decreased in the ovarian GCs and follicular fluid from females with PCOS. The ovulation-dependent ovarian expression of NTS and EGR1 transcripts was identified in a mouse superovulation model. First, we investigated the role of NTSR1-specific antagonist SR48692 in ovulation processes, such as cumulus expansion, oocyte maturation, and follicular rupture, *in vitro* and *in vivo*. We also established a PCOS-like mouse model to explore the role of NTS treatment in ameliorating polycystic ovarian changes. Furthermore, we investigated the mechanism of NTS/NTSR1/ERK/EGR1 signal axis in KGN cells, a human granulosa-like tumor cell line.

Materials and methods

Clinical samples

Ovarian GCs and follicular fluids were obtained during oocyte retrieval from patients with and without PCOS at the Center for Reproductive Medicine at Ren Ji Hospital, Shanghai Jiao Tong University School of Medicine, China. The participants gave their explicit consent prior to sample collection, which was performed in accordance with a protocol ratified by the Ethics Committee of Ren Ji Hospital, Shanghai Jiao Tong University School of Medicine. Females who met at least two of the following criteria for PCOS outlined by the updated Rotterdam consensus [28] were enrolled in the PCOS group: clinical and/or biochemical hyperandrogenism, oligo-ovulation and/or anovulation, and polycystic ovaries. Females with infertility caused by either tubal or male factors with regular menstrual cycles and normal ovarian morphologies were chosen as the control subjects. Tables S1 and S2 depict the clinical information of the patients, such as age, body mass index (BMI), and levels of the following hormones: LH, follicle-stimulating hormone (FSH), testosterone (T), estradiol (E2), and anti-Mullerian hormone (AMH). Following previous procedures [29], human ovarian GCs were collected from the follicular fluids of the patients. The follicular fluid was centrifuged to eliminate the cells and frozen at −80 °C for subsequent testing with an ELISA kit (Novus Biologicals, Littleton, CO, USA).

Cell culture

KGN cells were cultured in phenol red-free DMEM/F12 medium (Gibco, Grand Island, NY, USA) supplemented with 10% charcoal-stripped fetal bovine serum (FBS, Thermo Fisher Scientific, Waltham, MA, USA) and 1% antibiotics (Gibco). The cells were planted into six-well plates after being passaged every 2–3 days. After 24 h, the cells were incubated in serum-free DMEM/F12 for 6 h and exposed to either NTS (Tocris Bioscience, Bristol, UK) or U0126 (a selective inhibitor of MEK, 10 μmol/L, Selleck Chemicals, Houston, Texas, USA). For SR48692 (NTSR1-selective antagonist, R&D, Minneapolis, MN, USA) pretreatment, the cells were cultured with 10 μmol/L SR48692 in serum-free DMEM/F12 for 6 h and then stimulated for 5 or 30 min with NTS.

RNA extraction and quantitative real-time PCR

Total RNA was isolated from KGN cells or ovaries using the RNA extraction kit (Foregene Co., Ltd., Sichuan, China) and from oocytes or cumulus–oocyte complexes (COCs) using the RNeasy micro kit (Qiagen, Düsseldorf, Germany). After reverse transcription, the expression of target genes was analyzed by quantitative real-time polymerase chain reaction (qRT-PCR) utilizing the SYBR Green PCR master mix (Takara, Tokyo, Japan). The mRNA expression normalized to that of *Actb* was evaluated using the $2^{-\Delta\Delta Ct}$ approach. Table S3 presents the primer sequences that were used in this research.

Western blot assay

The ice-cold radioimmunoprecipitation test lysis buffer (Beyotime, Shanghai, China) containing phosphatase and protease inhibitors (Roche, Basel, Switzerland) was applied to lyse cells, COCs, and mouse ovaries. Equal amounts of proteins were loaded onto 10% SDS-PAGE for electrophoresis and then diverted to the nitrocellulose membrane (Millipore, Burlington, MA, USA). After blocking, the blots were sequentially incubated with primary and secondary antibodies. With the use of an enhanced chemiluminescence detection kit (Millipore), peroxidase-active protein bands were identified under the G-Box iChemi Chemiluminescence image capture equipment (Syngene, Haryana, India). The relative protein levels were analyzed by Image J. The antibody information is listed in Table S4.

Immunofluorescence staining

The KGN cells were cultured on chamber slides (Millipore) prior to immunofluorescent staining. After 5 or 30 min of NTS treatment, the cells were fixed with 4% paraformaldehyde at ambient temperature and permeabilized by 0.4% Triton X-100. After blocking, the cells were incubated with diluted primary antibodies, followed by incubation with the fluorescent secondary antibody. The nuclei were counterstained using DAPI, and a fluorescence microscope (Zeiss, Jena, Germany) was employed to capture images.

Animal models

Female C57BL/6 mice (Shanghai Model Organisms Center, Inc.) aged 21–23 days were randomly divided into several groups. All experiments were conducted in adherence to the National Institutes of Health Guide for the Care and Use of Laboratory Animals.

For the establishment of superovulation model, mice were injected intraperitoneally (i.p.) with 10 U of pregnant mare serum gonadotropin (PMSG, Sansheng Pharmaceutical, Ningbo, China) to stimulate follicle development. An ovulatory dose of 10 U hCG (Sansheng Pharmaceutical) was administered 48 h later. The mice were executed 48 h after the initiation of PMSG injection and 2, 4, 6, 8, 12, and 24 h after hCG administration. Ovaries were then excised, and the serum was collected to measure NTS levels.

For the other superovulation groups, mice were injected i.p. with SR48692 at a dosage of 10 mg/kg [30] or an equivalent volume of DMSO (Sigma–Aldrich) vehicle every 2 days for five times. Superovulation was induced in the last two treatments. The mice were sacrificed, and their ovaries were excised at different times after the injection. At 16 h after hCG treatments, COCs were isolated from the oviducts and the CCs were separated with hyaluronidase (embryo-tested grade, Sigma-Aldrich). The oocytes were then counted and imaged by a Zeiss microscope.

For the investigation of the lasting effects of SR48692, mice were given 10 mg/kg SR48692 i.p. or a vehicle every 2 days for 3 weeks. The estrous cycle was observed by vaginal cytological examinations for 12 consecutive days. The serum was collected to measure the sex hormones. Some of the ovaries were stained with hematoxylin and eosin (H&E) to discover abnormal changes, and the remaining ones were rapidly frozen and kept at −80 °C.

The PCOS mouse model was established following the protocol described by Qi *et al*. [31]. Three-week-old female C57BL/6J mice were procured from the Shanghai Model Organisms Center and acclimated under standard environmental conditions (20 °C, 12 h of light per day) with *ad libitum* access to water and rodent feed for 1 week. Afterward, the mice were randomly assigned to three groups: control group receiving daily subcutaneous (s.c.) injections of sesame oil (0.1 mL), DHEA group receiving daily s.c. injections of DHEA (D4000, Sigma–Aldrich, 6 mg per 100 g body weight, dissolved in 0.1 mL of sesame oil) to induce PCOS, and DHEA + NTS group receiving combined s.c. injections of DHEA and intraperitoneal (i.p.) injections of NTS (1 μg per 15 g body weight, R&D) for 20 consecutive days. Throughout the experimental period, the animals were weighed weekly. Vaginal smears were obtained daily at 09:00 am for 12 consecutive days before sacrifice. Microscopic analysis of the prevalent cell types in the smears revealed the estrous cycle phase: proestrus (characterized by a large number of nucleated epithelial cells), estrus (marked by cornified squamous epithelial cells), metestrus (exhibiting epithelial cells and leukocytes), and diestrus (dominated by a large number of leukocytes) [32]. Ovaries were collected for histological (H&E staining) and molecular (qRT-PCR analysis) examinations.

Ovarian histology

The ovaries were immediately extracted, fixed in 4% paraformaldehyde, placed in 70% ethanol, dehydrated, and soaked in paraffin. The tissues were serially sectioned at a thickness of 3 μm, and every tenth section was stained with H&E [33]. The slices were examined using a Zeiss microscope. The following criteria were classified and enumerated in accordance with established protocols [34,35]: small antral follicles (defined as an oocyte enveloped by over five layers of GCs and/or one or two tiny regions of follicular fluid), large antral follicles (characterized by a single large antral cavity), preovulatory follicles (identified as a large antral follicle containing an oocyte surrounded by CCs attached to a stalk of mural GCs), cystic follicles (manifesting as large fluid-filled cysts with an attenuated granulosa cell layer, scattered theca cell layer, and an oocyte not connected to the GCs, with a diameter > 400 μm), and corpora lutea (marked by a central chamber filled with blood and follicular fluid residue or conspicuous luteal cells). The categories of large antral follicles and preovulatory follicles were combined and collectively referred to as "large antral follicles".

Oocyte collection and culture

Female mice (3 weeks old) were given injections of 10 U PMSG for 46–48 h. The germinal-vesical (GV)-stage oocytes were then harvested by puncturing the large antral follicles with a micropipette in M2 medium (Sigma–Aldrich) and incubated in minidroplets of M16 medium (Sigma–Aldrich) coated with mineral oil (Sigma–Aldrich) at 37 °C in a 5% CO_2 environment.

siRNA knockdown

The GV-stage oocytes were microinjected with approximately 5–10 pL of *Egr1*-targeting or nontargeting siRNA (Genepharma, Shanghai, China). The effective level of siRNA was 25 μmol/L. The oocytes were detained at the GV stage for more than 12 h in M2 medium supplemented with 2.5 μmol/L milrinone. After thorough washing, the oocytes were moved to the milrinone-free M16 medium for 14 h to resume meiosis.

The KGN cells were transferred with siRNA by Lipofectamine 3000 (Invitrogen, Carlsbad, CA, USA) in accordance with the manufacturer's instructions and cultured for 48 or 72 h prior to the additional treatment. Table S5 shows the siRNA sequences.

Isolation of COCs

In brief, 3-week-old female mice were injected with 10 U of PMSG for 46–48 h. Immature COCs were then collected by puncturing follicles in the M2 medium. Ovulated COCs were also isolated from the oviducts 16 h after hCG administration. Total RNA was extracted from 100 COCs by utilizing an RNeasy micro kit (Qiagen, Düsseldorf, Germany), and each protein sample was lysed from 180–200 COCs.

Culture of COCs

COCs were obtained 46–48 h post-PMSG injection and cultured for 16 h with or without SR48692 to investigate the effect of the NTSR1 antagonist SR48692 on cumulus expansion and oocyte maturation *in vitro*. TCM-199 (Gibco) was employed as the maturation medium and added with 10% FBS, 1 μg/mL 17β-estradiol, 0.23 mmol/L sodium pyruvate, 0.05 IU/mL FSH, 0.05 IU/mL LH, and 10 ng/mL epidermal growth factor [36].

After the incubation period, the expansion degree was assessed using a scoring system ranging from 0 (no expansion) to 4 (maximal expansion). A score of 0 indicates no noticeable response, where CCs remain adherent to the culture medium and form a monolayer. A score of 1 represents the minimum detectable response, with only a small number of CCs attaching to the medium. A score of 2 signifies the initiation of expansion in the outer layers of CCs. A score of 3 indicates full expansion of all CC layers, except for the corona radiata. Finally, a score of 4 denotes maximal expansion, with the corona radiata and CCs fully expanded [37]. For the quantification of cumulus expansion, cumulus expansion index (CEI) was calculated as the average expansion value for each group. For example, in a group of 50 complexes, the expansion scores were distributed as follows: "0", 10 complexes; "1", 15 complexes; "2", 10 complexes; "3", 10 complexes; and "4", 5 complexes. The CEI for this group was computed as follows: $[(0 \times 10) + (1 \times 15) + (2 \times 10) + (3 \times 10) + (4 \times 5)] / 50 = 85/50 = 1.7$ [38].

For further assessment of oocyte maturation, the CCs were separated through a short incubation in M2 medium containing 300 μg/mL hyaluronidase [39]. Oocyte maturation was then assessed by scoring first polar body (PB1) extrusion.

Preparation of transcriptomic sequencing library and analysis of gene expression level

COCs were obtained 46–48 h after PMSG injection and cultured in the maturation medium with or without 100 μmol/L SR48692. After culturing for 4 or 16 h, the oocyte (10 oocytes per sample) or CC samples were separated from the control and SR48692-treated groups for transcriptomic sequencing (RNA-seq). All the oocyte samples were promptly lysed with 10 μL of lysis buffer and utilized for cDNA synthesis via the published Smart-

Seq2 protocol [40], and the CC samples were subjected to RNA purification and subsequent cDNA synthesis using a SMART-Seq® HT Kit (Clontech, Tokyo, Japan).

Library preparation and sequencing were carried out on the NovaSeq 6000 platform (Illumina, Inc., San Diego, CA, USA). The sequencing reads were mapped to the mouse genome (GRCm38) utilizing Hisat2 (version 2.0.4). The expression of every gene was quantified with normalized fragments per kilobase of transcript per million mapped reads (FPKM). DEGs were analyzed by edgeR with the standard of a q-value < 0.05 and a fold change > 2 or < − 2. Gene ontology (GO) was utilized to annotate biological functions, and the Kyoto Encyclopedia of Genes and Genomes (KEGG) was used to identify the relevant pathways. GENESIS BIO (Shanghai, China) helped complete the sequencing and annotation of the data.

Mitochondrial distribution analysis

For the mitochondrion distribution analysis, oocytes were cultured in M2 containing 200 nmol/L Mito-Tracker Red CMXRos (Beyotime) for 30 min. After being washed three times with the M2 medium, the oocytes were transferred onto glass slides and examined with a fluorescence microscope (Zeiss).

Determination of intracellular ROS levels

The intracellular ROS levels of COCs were tested by 2′,7′-dichlorofluorescin diacetate (DCFH-DA) staining (Sigma-Aldrich). In brief, COCs from each group were moved to a solution containing 10 μmol/L DCFH-DA and 0.3% PVP-DPBS. After 30 min of incubation at 37 °C in the dark, COCs were rinsed three times with 0.3% PVP-DPBS and imaged by the fluorescence microscope (Zeiss). Image J was employed to quantify the fluorescence intensity.

ATP measurement

The intracellular ATP concentrations of oocytes and COCs were measured using an ATP determination kit in compliance with the manufacturer's guidelines (Invitrogen, San Diego, CA, USA).

Electron microscopy

COCs were obtained 46–48 h post-PMSG injection, cultured for 16 h with or without SR48692, fixed in 2.5% glutaraldehyde (pH 7.0–7.5) for 2–4 h, post-fixed with 1% osmic acid and soaked in Epon 812 after dehydration. Ultrathin sections (60 nm) were cut by an ultramicrotome (UC7, Leica Microsystems, Vienna Austria), dyed using uranyl acetate and lead citrate, and imaged with the Hitachi HT7700 electron microscopy (Hitachi, Tokyo, Japan).

Serum analysis

The serum samples were centrifuged at 2500 rpm. for 20 min at 4 °C and then frozen at –80 °C for further analyses. ELISA kits were used to test the concentration of testosterone (DEV9911, Demeditec Diagnostics, Germany), progesterone (DEV9988, Demeditec Diagnostics), and NTS (orb565418, Biorbyt, UK) in mice.

Statistical analysis

All results are presented as the mean ± SD or SEM. GraphPad Prism and IBM SPSS Statistics were used for statistical analyses. All the data were tested for normality. Two-tailed Student's t-test was applied to analyze the statistical differences between the two groups. One-way ANOVA followed by Dunnett's multiple comparisons test was performed to analyze data from three or more experimental groups. $P < 0.05$ was set as the statistical significance threshold.

Results

NTS expression was decreased in PCOS

Considering that NTS is associated with obesity and fat metabolism [41,42], we recruited females with PCOS and controls with similar BMI to eliminate the influence of obesity in these two groups. Compared with control females, the patients with PCOS had significant higher basal LH, basal T, and AMH (Tables S1 and S2). The NTS expression in ovarian GCs and follicular fluids was substantially decreased in the PCOS group compared with that in the control group (Fig. 1A and 1B), indicating that NTS may play a crucial role in PCOS development.

***In vivo* regulation of ovarian NTS expression in mouse models**

Accumulating evidence suggests that NTS participates in the central control of the preovulatory rise of LH [43]. Considering that NTS antibody-injected follicles fail to ovulate [14], we suspected that decreased follicular NTS concentrations may be responsible for anovulation and poor oocyte quality in PCOS. To investigate ovarian NTS expression during ovulation *in vivo*, we chose the PMSG-induced/hCG-triggered immature mouse superovulation model. NTS abundance in ovaries and serum reached a peak 6 h after hCG injection and returned to baseline 12 h later (Fig. 1C–1E). In addition, NTS expression was higher in hCG-triggered ovulated COCs than in PMSG-primed immature COCs (Fig. 1F–1H). These results

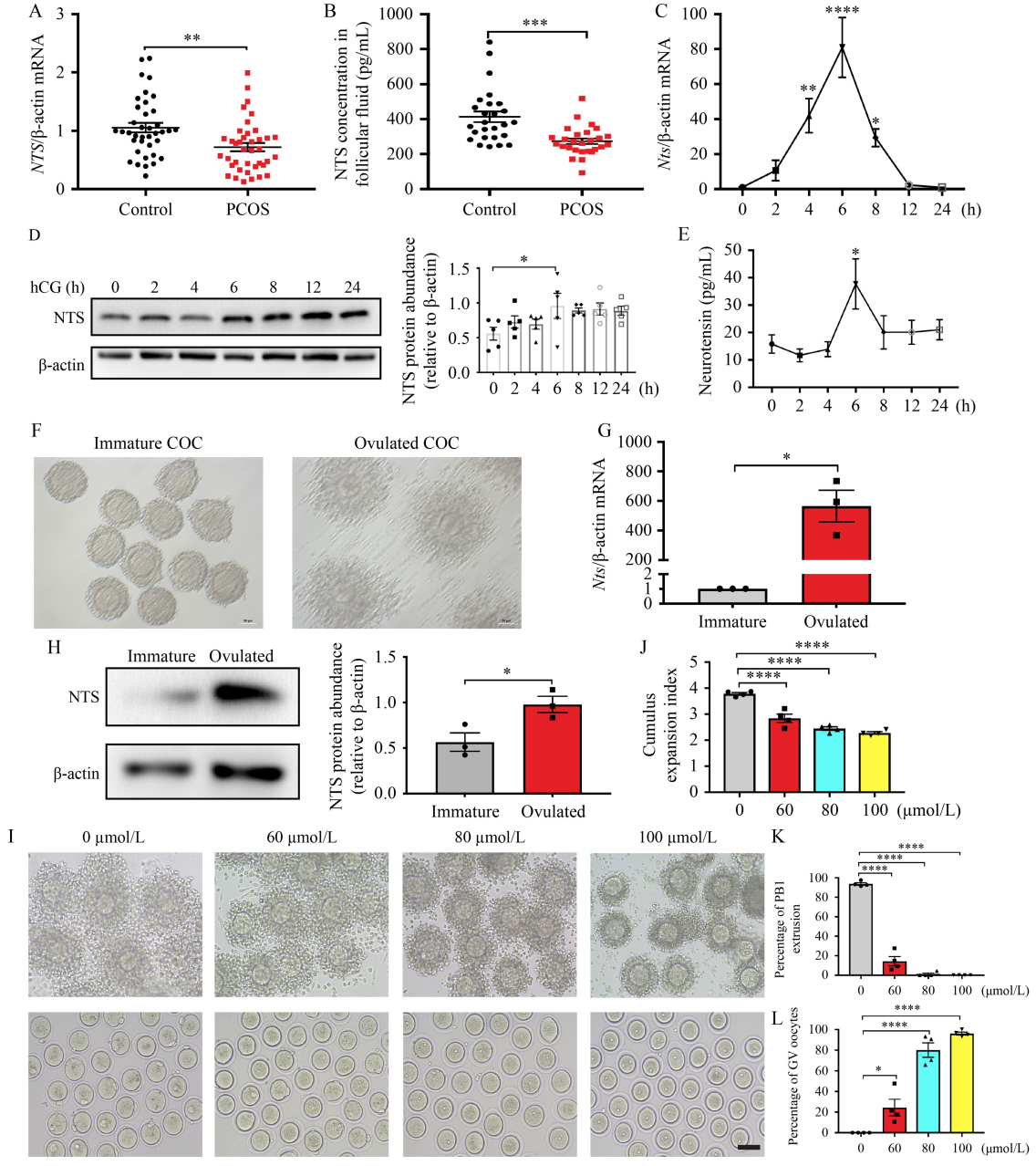

Fig. 1 Neurotensin (NTS) had decreased expression in polycystic ovary syndrome (PCOS) and played an important role in ovulation. (A) qRT-PCR detection of *NTS* expression in ovarian granulosa cells (GCs) from 38 normal controls and 39 patients with PCOS. (B) ELISA for NTS in the follicular fluid from 26 normal controls and 27 patients with PCOS. (C–E) Immature female mice were primed with 10 U of pregnant mare serum gonadotropin (PMSG), followed by the administration of 10 U of human chorionic gonadotropin (hCG) at the designated time points (hours). (C) qRT-PCR analysis of *Nts* mRNA expression pattern in superovulated mouse ovaries (n = 4–6). (D) Whole ovarian protein was isolated from superovulated mice and examined by Western blot analysis using antibodies against NTS (n = 5). (E) Serum NTS levels in superovulated mice at different times after hCG stimulation as detected by ELISA (n = 4–5). (F) Representative images of immature cumulus–oocyte complexes (COCs) and ovulated COCs. Scale bar: 50 μm. Immature COCs were obtained from large antral follicles in mice primed with PMSG for 48 h, indicating no expansion of cumulus cells surrounding a germinal-vesicle (GV) oocyte. Ovulated COCs were isolated from the oviduct in mice injected with PMSG for 48 h following hCG for 16 h, showing the complete expansion of cumulus cells surrounding a MII oocyte. (G) *Nts* was quantified by qRT-PCR in immature and ovulated COCs (n = 3). (H) Protein levels of NTS in immature and ovulated COCs (n = 3). (I–L) COCs were obtained 46–48 h post-PMSG injection and cultured for 16 h with the indicated concentrations of NTSR1 antagonist SR48692 or with control medium. (I) Effects of SR48692 on cumulus expansion and oocyte meiotic maturation. Scale bar: 100 μm. (J) Degree of cumulus expansion was evaluated between the control and SR48692-treated groups according to a subjective scoring system, a scale of 0 (no expansion) to 4 (maximal expansion). For each treatment group, a mean cumulus expansion index was calculated. (K, L) First polar body (PB1) extrusion rates and GV rates between the control and SR48692-treated groups. Each point reported in the figures is the mean ± SEM of 30 or more COCs analyzed in four separate experiments. Data are presented as the mean ± SEM. *P < 0.05, **P < 0.01, ***P < 0.001, ****P < 0.0001.

suggest that the NTS expression in ovaries has an ovulation-dependent pattern, which may be crucial for cumulus expansion and meiotic maturation.

NTSR1 antagonist SR48692 inhibited cumulus expansion and oocyte meiotic maturation in a dose-dependent manner

To explore the role of NTS/NTSR1 in cumulus expansion and oocyte maturation, the two important steps in ovulation, we collected the unexpanded COCs from the mice injected with PMSG for 46–48 h and incubated them with increasing doses of NTSR1 antagonist SR48692 in the maturation medium. After 16 h of culture, the cumulus expansion degree was evaluated. In the control group, the CCs underwent maximal expansion. By contrast, SR48692 inhibited cumulus expansion in a dose-dependent manner, suggesting that NTS/NTSR1 signaling is important for cumulus expansion (Fig. 1I and 1J). Oocyte maturation was also observed by scoring the PB1 extrusion after CC isolation. Meiotically arrested oocytes were identified by the presence of nuclear structures called germinal vesicle (GV). We observed that SR48692 supplementation significantly reduced PB1 extrusion in a dose-dependent manner (Fig. 1I and 1K). In addition, 100 μmol/L SR48692 completely arrested oocytes at the GV stage, demonstrating that excess SR48692 may disrupt meiotic maturation (Fig. 1I and 1L).

SR48692 treatment influenced oocyte energy metabolism during meiotic maturation

Immature oocytes in the GV stage resume meiosis, characterized as the germinal vesicle breakdown (GVBD). This phenomenon is a milestone event of oocyte maturation [44]. To elucidate the potential mechanisms underlying the inhibition of oocyte maturation by excess SR48692, we performed RNA-seq analyses using smart-seq 2 of oocytes incubated for 4 h in the maturation medium with or without SR48692 (Fig. 2A). The oocytes in the control group induced GVBD, and those in the SR48692 group were absolutely blocked in the GV phase (Fig. 2A). Q-value < 0.05 and fold change > 2 or < −2 were chosen as cutoffs for DEG analyses. A total of 1783 genes were significantly altered in the SR48692-treated oocytes, with 451 genes elevated and 1332 reduced. Among them, the genes related to oocyte maturation, such as betacellulin (*Btc*), and ribonuclease III (*Dicer1*), were differentially expressed (Fig. 2B).

GO analysis revealed that multiple DEGs were enriched in the functions of mitochondria and ribosomes (Fig. S1). To further confirm the causative pathways in SR48692 supplementation, we employed KEGG to analyze the DEGs and found that many pathways related to oxidative phosphorylation, glutathione metabolism, and amino acid and fatty acid metabolism were significantly enriched (Fig. 2C). Moreover, significant downregulation was observed for most of the genes associated with the oxidative phosphorylation pathway (Fig. 2D), which is involved in the respiratory chain of the mitochondria (Fig. S2).

Identification of the targets of SR48692 that inhibited COC expansion in CCs

To further determine the cause of COC expansion defection after SR48692 supplementation, we subjected CCs cultured for 16 h with or without SR48692 to perform RNA-seq analyses by smart-seq 2 (Fig. 2A). The CCs in the control group reached full expansion. However, these impacts were significantly inhibited by the supplementation of SR48692. A total of 4148 genes in CCs exhibited striking differences between the two groups, with 1685 genes elevated and 2463 genes reduced (Fig. S3A and S3B) in the SR48692 group. Many genes related to cumulus expansion, such as peroxiredoxin 2 (*Prdx2*), were significantly reduced (Fig. S3A). KEGG analyses revealed that majority of the DEGs were involved in steroid/unsaturated fatty acid/amino acid biosynthesis, glutathione/cholesterol/amino acid/pyruvate metabolism, glycolysis, and ovarian steroidogenesis (Figs. S3C and S4). Moreover, many genes associated with the oxidative phosphorylation pathway were significantly downregulated (Fig. S5).

SR48692 inhibited the metabolic codependence of oocytes and surrounding CCs

The bidirectional communication between oocytes and their companion CCs is important for the final stages of maturation prior to ovulation [45]. We next analyzed the significant overlap between them after SR48692 treatment. Venn diagrams revealed 287 shared transcripts that were upregulated (18.82%) or downregulated (81.18%) in oocytes and CCs (Fig. 2E). GO and KEGG analyses of the commonly downregulated genes revealed that they were enriched in several metabolic pathways, including oxidative phosphorylation, glutathione metabolism, glycolysis, and amino acid and fatty acid metabolism (Figs. 2F and S6).

Oocytes lack necessary enzymatic systems for glycolytic and cholesterol formation and key transporters for specific amino acids, both of which are essential for energy production and meiotic maturation. Hence, they need to obtain these products from CCs. Proper coordination of these metabolic processes between oocyte and CCs is crucial for oocyte maturation [46]. We found that the transcripts related to amino acid synthesis and metabolism, cholesterol metabolism, pyruvate metabo-

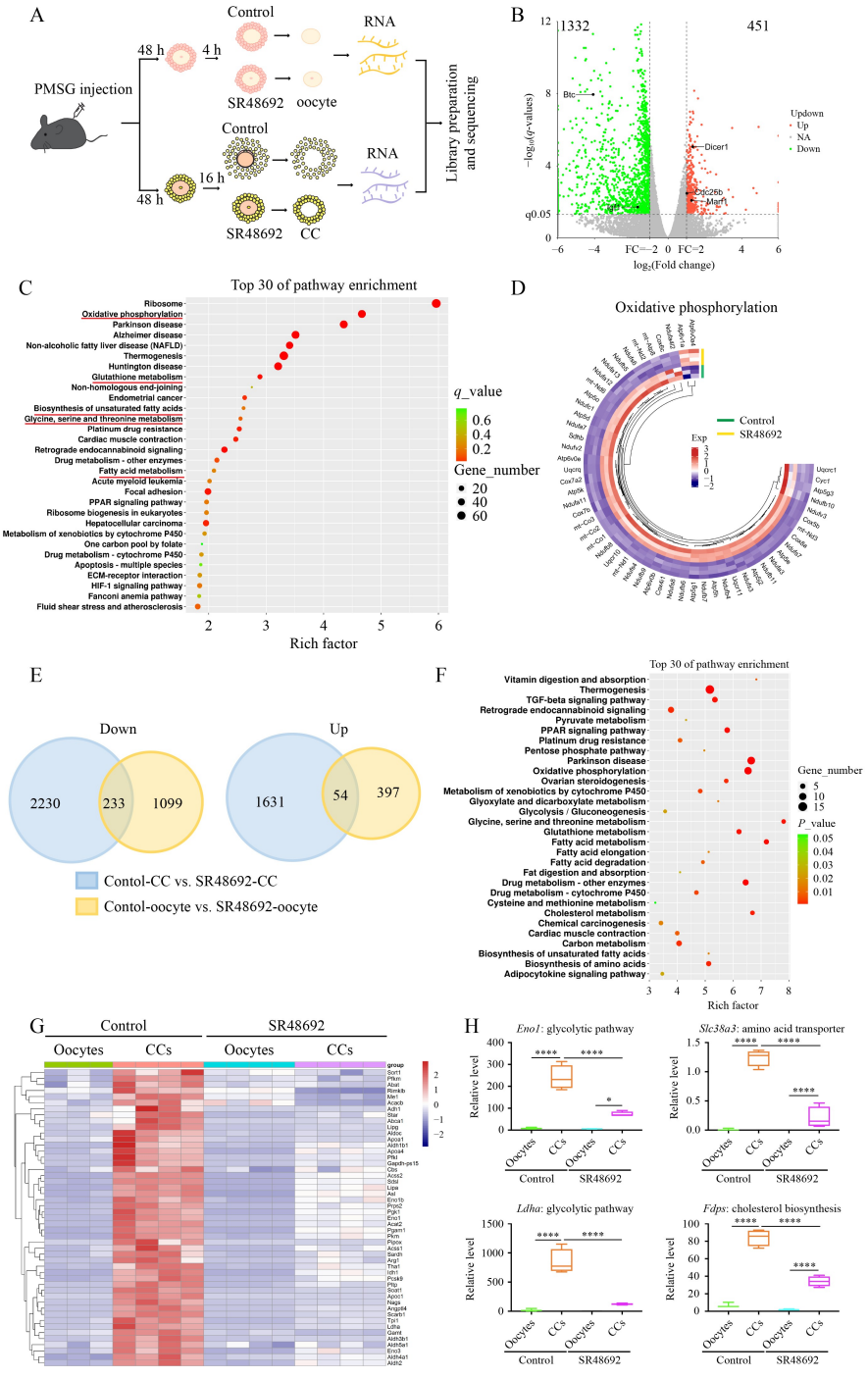

Fig. 2 NTS receptor 1 (NTSR1) antagonist SR48692 inhibited the metabolic codependence of oocytes and surrounding cumulus cells (CCs). (A) Schematic of the study workflow. Cumulus–oocyte complexes (COCs) were obtained 46–48 h after pregnant mare serum gonadotropin (PMSG) injection and cultured in the maturation medium with or without 100 μmol/L SR48692. After being cultured for 4 h, the oocyte samples (10 oocytes per sample) were separated from the control and SR48692-treated groups for RNA-seq. After being cultured for 16 h, the CC samples were separated for RNA-seq. (B) Corresponding volcano plot of SR48692-treated oocytes versus controls showing 451 upregulated (fold change > 2, q-value < 0.05, red) and 1332 downregulated (fold change < − 2, q-value < 0.05, green) genes. (C) Top 30 signaling pathways of differentially expressed genes (DEGs) in Kyoto Encyclopedia of Genes and Genomes (KEGG) enrichment analysis between control and SR48692-treated oocytes. (D) Changes in DEG levels in oxidative phosphorylation between control and SR48692-treated oocytes. (E) Venn diagrams showing the overlap of downregulated (fold change < − 2, q-value < 0.05) and upregulated (fold change > 2, q-value < 0.05) transcripts in SR48692-treated oocytes and CC samples. (F) KEGG analyses of the overlap in transcripts that were downregulated in SR48692-treated CCs and oocytes. (G) Heat maps of the relative expression of the indicated genes in amino acid synthesis and metabolism, cholesterol metabolism, pyruvate metabolism, and glycolysis in the four groups. Each box corresponds to a different sample. (H) Differential gene expression associated with metabolic cooperation between oocytes and CCs. Data are shown as means ± SEM. *P < 0.05, ****P < 0.0001.

lism, and glycolysis were upregulated in CCs compared with those in oocytes in the control group. However, these transcripts were lower in the SR48692-treated CCs (Fig. 2G). In addition, some genes involved in the metabolic cooperation of oocytes and surrounding CCs were significantly altered. For example, the transcripts encoding key enzymes in the glycolytic pathway (including α-enolase 1 (*Eno1*) and lactate dehydrogenase A (*Ldha*)), amino acid transport (solute carrier family 38 member 3 (*Slc38a3*)), and pathway of cholesterol synthesis (farnesyl diphosphate synthase (*Fdps*)) were strongly expressed in CCs but nearly undetectable in oocytes. All of these transcripts were dramatically reduced in the SR48692-treated CCs (Fig. 2H). These results indicate that SR48692 may prevent cumulus expansion and oocyte maturation by inhibiting the metabolic cooperation between CCs and oocytes.

SR48692 treatment induced mitochondrial dysfunction in oocytes and CCs

Given that most of the downregulated genes were enriched in oxidative phosphorylation (Fig. 3A) and the important role of mitochondria is to generate ATP by oxidative phosphorylation, we next examined the mitochondrial function. As nuclear maturation occurs in oocytes, the mitochondrial DNA copy number strikingly increases and the distribution of mitochondria changes dramatically [47]. Thus, we evaluated the mitochondrial content in oocytes with Mito-Tracker Red CMXRos. SR48692 treatment blocked the spatial remodeling of mitochondria in the cytoplasm compared with that in the control group (Fig. 3B). Considering that mitochondrial damage would increase ROS, we performed DCFH-DA staining to detect the ROS levels of COCs in each group. Fluorescence scanning and intensity metrics demonstrated that SR48692 treatment significantly increased ROS deposition in COCs (Fig. 3B and 3C). In addition, the ATP levels of oocytes and COCs treated with SR48692 were also lower than those of the control groups (Fig. 3D). Electron microscopy examination was conducted to further explore the accumulation of impaired mitochondria. No evident structural alteration of mitochondria was found in the control group. By contrast, the mitochondria of the oocytes and CCs exposed to SR48692 for 16 h showed abnormal swelling and crista disruption (Fig. 3E and 3F). This observation suggests that NTS/NTSR1 plays a crucial role in cumulus expansion and oocyte maturation by controlling the mitochondrial function in oocytes and surrounding CCs.

***In vivo* and *in vitro* analyses of EGR1 in the ovulatory process**

Among the enriched candidates detected by RNA-seq analyses, we identified EGR1, a zinc-finger transcription factor that participates in ovulatory function [25]. RNA-seq results showed that *Egr1* was dramatically decreased in the SR48692-treated CCs (Fig. 4A), which was further confirmed in the COCs by qRT-PCR (Fig. 4B). The ERK1/2 pathway is believed to activate EGR1 [26]. In line with these findings, we found that an ovulatory dose of hCG caused the fast and transitory expression of ERK1/2 phosphorylation and EGR1 2–4 h after injection (Fig. 4C and 4D). Furthermore, the protein level of EGR1 was higher in ovulated COCs than in immature COCs (Fig. 4E).

We examined whether EGR1 participates in oocyte maturation in mice by silencing its expression in GV oocytes using the small interfering RNA (siRNA) (Fig. 4F). We found that the PB1 extrusion rate in the *Egr1*-depleted oocytes was reduced compared with that in the control group (Fig. 4G and 4H). This evidence illustrates that EGR1 participates in ovulation, and inadequate EGR1 results in aberrant oocyte development.

Effect of NTSR1 blockade on ovulation *in vivo*

Basing on the above results, we further explored the impact of NTS/NTSR1 on ovulation *in vivo* by utilizing SR48692. Immature female mice were injected i.p. with 10 mg/kg SR48692 every 2 days for five times. Superovulation was concurrently induced in the last two treatments (Fig. 5A). The mice were sacrificed at 0, 4, and 16 h post-hCG. No significant variation in body weight was observed for the two groups (Fig. 5B).

The ERK/EGR1 pathway could potentially participate in ovulation control. GO analyses of the commonly downregulated genes showed that SR48692 could negative regulate the ERK1 and ERK2 cascade (Fig. S6). We next compared ERK/EGR1 expression in ovaries between the two groups. As expected, the relative ovarian mRNA and protein abundance of EGR1 was upregulated from 0 to 4 h post-hCG in vehicle-treated mice, but this dramatic increase was abolished in SR48692-treated mice. Concurrently, SR48692 inhibited hCG-induced ERK1/2 phosphorylation (Fig. 5C and 5D).

The number of ovulated oocytes from the oviducts was counted 16 h after hCG treatment to confirm the ovulation-blocking activity of SR48692. Injection with SR48692 resulted in lower numbers of retrieved total oocytes per mouse (Fig. 5E and 5F). Moreover, we examined ovarian morphology for further evaluation. At 16 h after hCG administration, the ovaries from the control group consisted of multiple ruptured follicles replete with corpora lutea. Meanwhile, the hCG + SR48692-treated mouse ovaries exhibited many dominant follicles that failed to rupture (Fig. 5E). To further estimate corpus lutea function, we examined serum progesterone levels in superovulated mice with or without

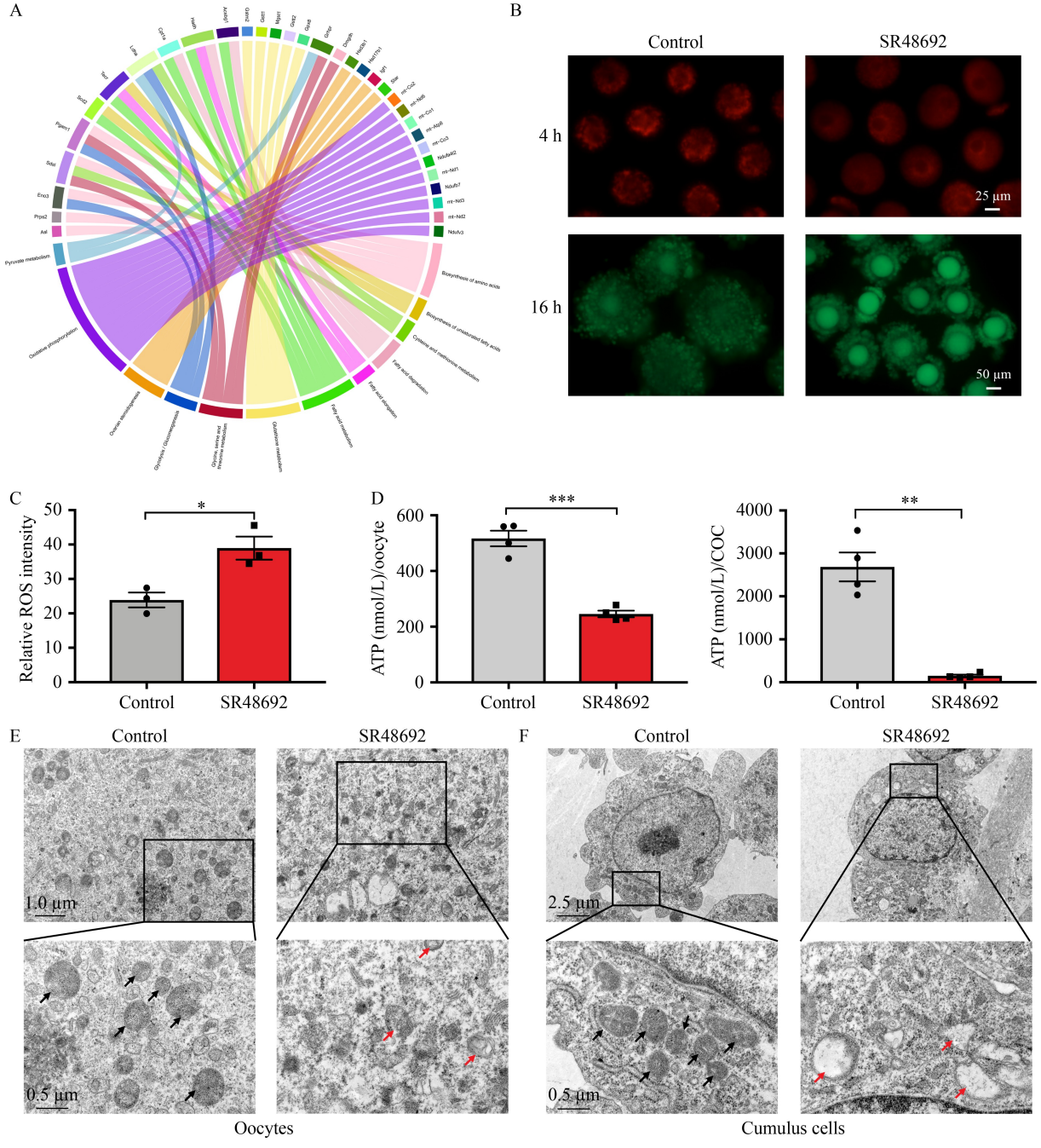

Fig. 3 SR48692 treatment induced mitochondrial dysfunction in oocytes and cumulus cells. (A) Network of genetic interactions of genes involved in enriched pathways. (B) Mitochondrial distribution in oocytes (red, scale bar: 25 μm) and reactive oxygen species (ROS) accumulation in cumulus–oocyte complexes (COCs) (green, scale bar: 50 μm). (C) Relative fluorescence intensity was analyzed by Image J software. (D) Intracellular adenosine triphosphate (ATP) concentrations in the oocytes and COCs of the control and SR48692-treated groups. (E, F) Electron microscopy observation of the mitochondrial morphology in the control and SR48692-treated COCs. Black arrows mean normal mitochondria, and red arrows mean damaged mitochondria. Data are presented as the mean ± SEM. *$P < 0.05$, **$P < 0.01$, ***$P < 0.001$.

SR48692. The serum progesterone levels were prominently elevated from 0 to 16 h post-hCG in vehicle-treated mice. However, concurrent injection with SR48692 led to a reduction in serum progesterone compared with that in the controls at 16 h post-hCG (Fig. 5G).

Effect of SR48692 treatment duration on mouse ovaries

Considering that SR48692 injection for five times caused diminished superovulatory responsiveness, we examined whether the lasting consequences of SR48692 would

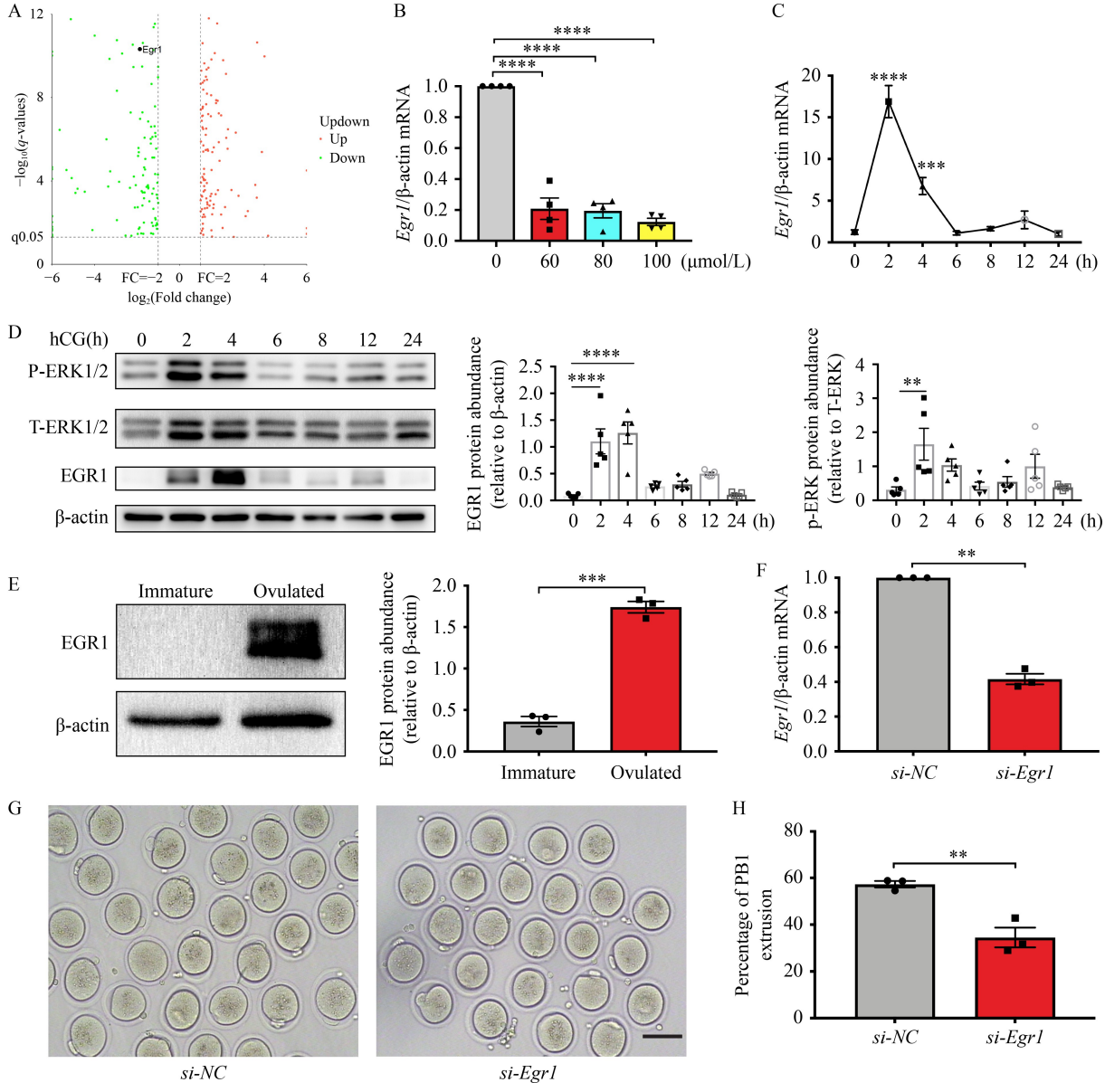

Fig. 4 As a critical downstream mediator of NTS/NTSR1, early growth response 1 (EGR1) participated in the ovulation process. (A) Corresponding volcano plot of different transcription factors in control versus SR48692-treated cumulus cells. Transcription factors that increased or decreased by more than two fold are highlighted in red or green, respectively. (B) qRT-PCR analysis of the *Egr1* mRNA expression pattern in COCs treated with different SR48692 concentrations ($n = 4$). (C) qRT-PCR analysis of *Egr1* mRNA expression in superovulated mouse ovaries ($n = 4$–6). (D) Protein levels of EGR1, phospho-ERK1/2, and total ERK-1/2 in the ovaries of superovulated mice ($n = 5$). (E) Protein levels of EGR1 in immature and ovulated COCs ($n = 3$). (F) Depletion of *Egr1* in oocytes was determined by qRT-PCR. (G) Representative images of oocyte maturation after *Egr1* depletion. Scale bar: 100 μm. (H) PB1 extrusion rates between the control and *Egr1* depletion groups. Data are presented as the mean ± SEM. $^{**}P < 0.01$, $^{***}P < 0.001$, $^{****}P < 0.0001$.

induce ovulatory dysfunction in a mouse model. Therefore, we injected mice i.p. with SR48692 (10 mg/kg) or vehicle every 2 days for 3 weeks. No difference was found in ovarian weight (Fig. 6A) and body weight (Fig. 6B) between two groups during the entire observation period.

Estrous cycles were observed by daily inspecting vaginal smears to further estimate reproductive functions. The SR48692-treated mice exhibited disrupted estrous cyclicity with prolonged time in estrus and lessened time in proestrus (Fig. 6C and 6D). The ovarian histology of SR48692-treated mice exhibited anomalies associated with the oligo-ovulation phenotype, with less corpora lutea compared with those in the controls (Fig. 6E and 6G). Moreover, we measured circulating progesterone between the two groups and discovered lower levels in the SR48692-treated mice. However, the differences in testosterone levels did not reach statistical significance

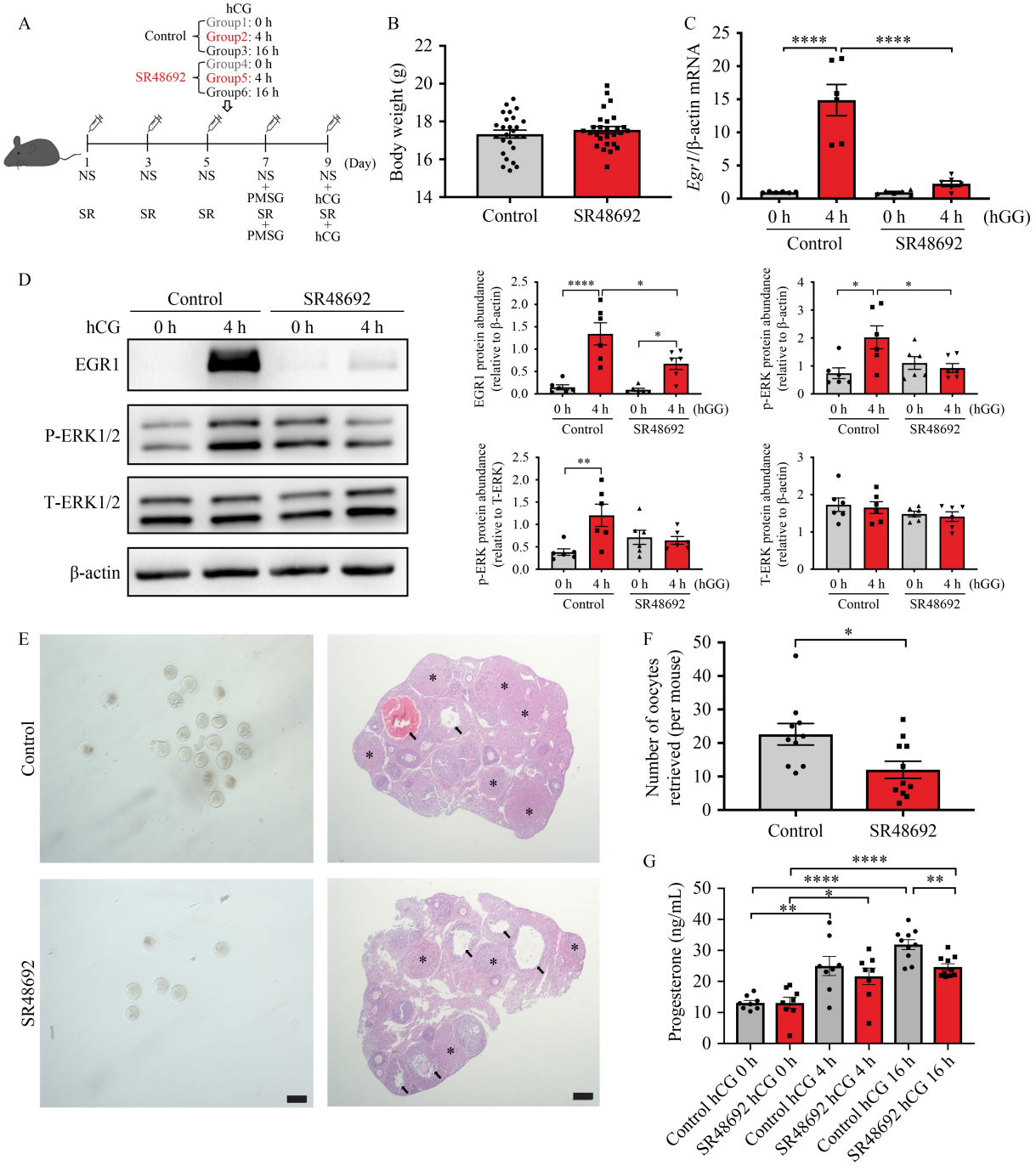

Fig. 5 Effect of NTSR1 antagonist SR48692 coinjection on superovulated mice. (A) Schematic of the experimental design wherein immature female mice were subjected to different managements of i.p. injections every 2 days for a total of 5 times (NS: normal saline; SR: SR48692, 10 mg/kg) and split into six treatment groups: Control + hCG 0 h, Control + hCG 4 h, SR48692 + hCG 0 h, SR48692 + hCG 4 h, Control + hCG 16 h, and SR48692 + hCG 16 h. (B) Body weight of control and SR48692-treated mice (Control: $n = 26$; SR48692: $n = 27$). (C) qRT-PCR analysis of *Egr1* mRNA expression pattern in superovulated mouse ovaries at 0 and 4 h post-hCG injection ($n = 6$ mice per group). (D) Western blot analysis of EGR1, phospho-ERK1/2, and total ERK-1/2 levels in superovulated mouse ovaries at 0 and 4 h post-hCG injection ($n = 6$ mice per group). (E) Representative images of oocytes retrieved per mouse (left, scale bar: 100 μm) and histological examinations (right, scale bar: 200 μm) of the impact of SR48692 coinjection on superovulated mice 16 h after hCG administration. Right: Thick arrows indicate unruptured follicles, and asterisks indicate corpora lutea. (F) Numbers of retrieved oocytes per mouse (control: $n = 10$; SR48692: $n = 11$). (G) Serum progesterone levels at 0, 4, and 16 h post-hCG detected by ELISA ($n = 8–10$ mice per group). Data are presented as the mean ± SEM. $^*P < 0.05$, $^{**}P < 0.01$, $^{****}P < 0.0001$.

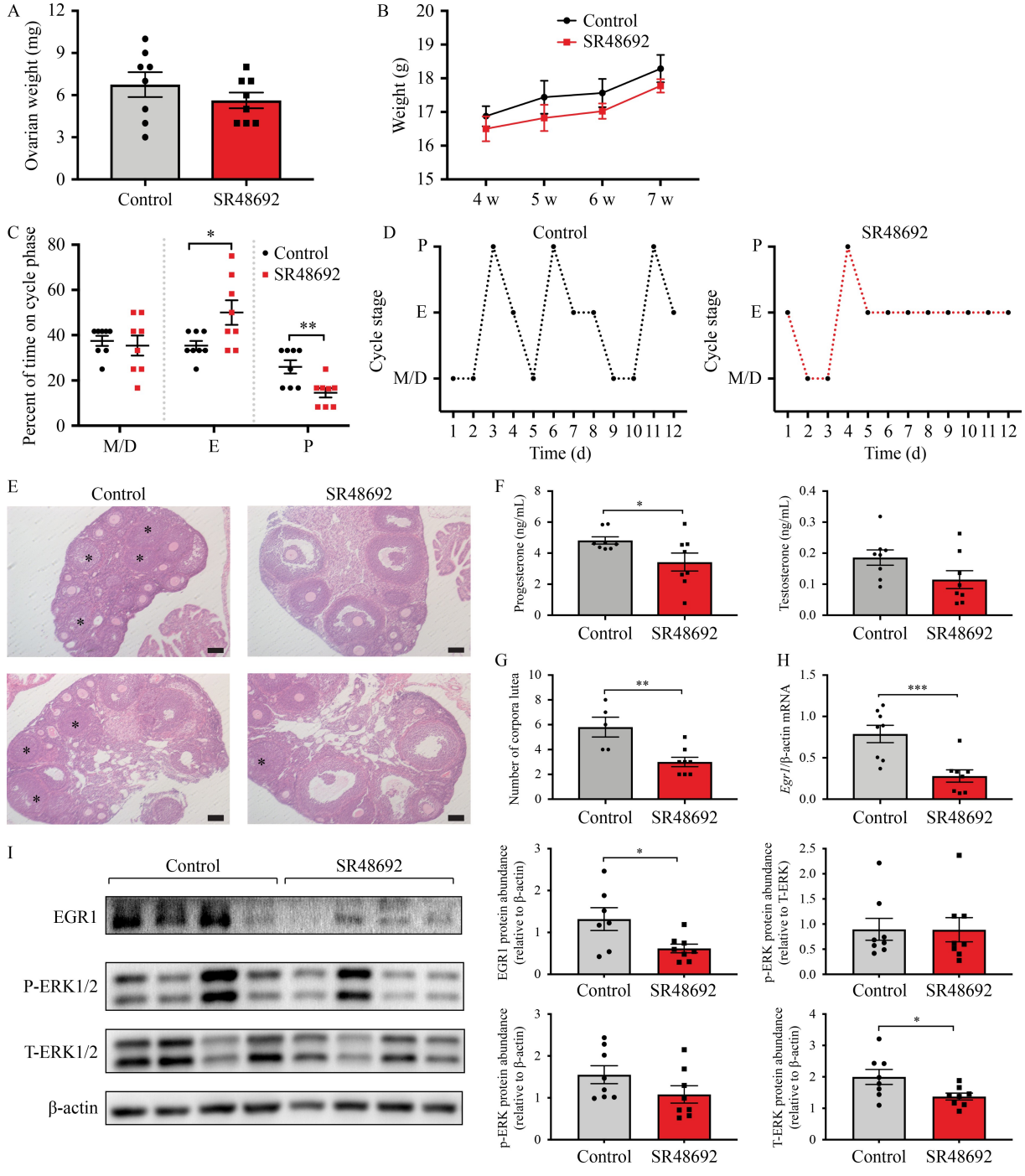

Fig. 6 Long-term effects of the NTSR1 antagonist SR48692 caused ovulatory dysfunction *in vivo*. Immature female mice were injected i.p. with SR48692 (10 mg/kg) or vehicle every 2 days for 20 days. (A) Ovarian weight. (B) Body weight between the control and SR48692-treated mice (n = 8 mice per group). (C) Quantitative analysis of ovarian cyclicity (n = 8 mice per group). Vaginal cytology was assessed for 12 days. M/D: metestrus and diestrus; P: proestrus; E: estrus. (D) Representative estrous cyclicity. (E) Hematoxylin and eosin (H&E) staining of ovaries. The corpora lutea are indicated by asterisks. Scale bar: 100 μm. (F) Serum progesterone and testosterone levels (n = 8 mice per group). (G) Quantitative analysis of corpora lutea (control: n = 5; SR48692: n = 8). (H) *Egr1* mRNA expression in ovaries (n = 8 mice per group). (I) Western blot analysis of EGR1, phospho-ERK1/2, and total ERK-1/2 levels in ovaries (n = 7–8 mice per group). Data are represented as the mean ± SEM. $^{*}P < 0.05$, $^{**}P < 0.01$, $^{***}P < 0.001$.

(Fig. 6F).

We also explored the role of ERK1/2 and EGR1 in the treatment groups. The expression of EGR1 and total ERK1/2 decreased in the SR48692-treated ovaries (Fig. 6H and 6I). These findings support the hypothesis that the treatment duration of NTSR1 antagonists causes

ovulatory dysfunction via attenuating ERK/EGR1 signaling.

NTS partially improved polycystic ovarian changes in PCOS-like mice

Given our findings of low NTS expression in follicular fluids and ovarian GCs from PCOS subjects combined with the *in vivo* and *in vitro* results from animal models, we hypothesized that NTS administration might ameliorate ovulatory abnormalities in mice with PCOS. Thus, a PCOS-like mouse model induced by DHEA injection was chosen to estimate the impacts of NTS on PCOS pathophysiology. The mice were randomly divided into three groups of control, DHEA, and DHEA + NTS, which were given vehicle, DHEA (6 mg/100 g body weight), and the same DHEA with NTS (1 μg/15 g body weight), respectively. All animals were injected for 20 successive days.

The DHEA-injected mice gained more weight compared with the control group. NTS administration did not ameliorate the DHEA-induced elevation in weight gain (Fig. 7A). The control mice showed a typical estrous cycle between 4 and 5 days (Fig. 7B and 7C). By contrast, the DHEA-injected animals displayed severely disturbing estrous cyclicity and most of them exhibited constant estrus (Fig. 7B and 7D). NTS treatment partially improved DHEA-induced acyclicity (Fig. 7B and 7E).

From a histological view, the DHEA group displayed aberrant ovarian morphology with multiple cyst-like appearances of follicles compared with the controls (Fig. 7F and 7G). The DHEA + NTS group exhibited fewer fluid-filled cystic follicles than the DHEA-treated mice (Fig. 7F and 7G). We observed an increase in the number of small antral follicles in the DHEA group compared with that in the control group, indicating a greater proportion of follicles in a growth-arrested state in PCOS-like mice (Fig. S7A). Meanwhile, the large antral follicles and corpus luteum counts were lower in the DHEA group than in the control group, suggesting reduced oocyte ovulation in PCOS-like mice (Fig. S7B and S7C). However, these trends were partially alleviated following NTS administration (Fig. S7A and S7C). Furthermore, we evaluated the mRNA expressions of *Nts*, *Ntsr1*, and *Egr1* in the ovaries and found that they were significantly downregulated in the DHEA mice compared with those in the control group. NTS treatment effectively upregulated the expression of *Nts* and *Ntsr1*, and tended to increase the expression of *Egr1* (Fig. S7D–S7F). These results reveal that NTS can partially ameliorate DHEA-induced ovarian anomalies in mice.

NTS-induced EGR1 expression was mediated via NTSR1-ERK1/2 in KGN cells

As previously demonstrated in animal models, NTS/NTSR1 might participate in ovulation-related events through the ERK/EGR1 signaling pathway. We subsequently verified the molecular mechanism in KGN cells, a human granulosa-like tumor cell line. The results illustrated that NTS addition to serum-starved KGN cells markedly increased ERK1/2 phosphorylation in a time- and dose-dependent manner (Figs. 8A, 8B, and S8). Consistent with this finding, immunofluorescence staining demonstrated that phosphor-ERK1/2 translocated into the nucleus within 5 min (Fig. 8C). To determine whether NTS activates ERK through the NTSR1 signaling pathway, we treated cells with 10 μmol/L SR48692 in serum-free DMEM/F12 for 6 h and challenged them for 5 min with NTS. SR48692 markedly suppressed the elevation in ERK phosphorylation triggered by 100 nmol/L NTS. In addition, SR48692 alone could significantly inhibit total ERK (Figs. 8D and S8).

Time-course analysis revealed that 100 nmol/L NTS stimulated EGR1 expression within 30 min and then returned to the initial state after 2 h (Figs. 8E and S8). Exposure to various NTS concentrations positively upregulated the EGR1 protein level of KGN cells in a dose-dependent manner (Figs. 8F and S8). NTS increased the robust nuclear accumulation of EGR1 within 30 min (Fig. 8H). These results indicate that NTS speedily and transiently increases EGR1 expression and induces its nuclear localization. Similarly, 10 μmol/L SR48692 significantly abolished the ability of NTS to induce EGR1 (Figs. 8G and S8).

Given that the MAPK pathway is essential for EGR1 gene transcription in response to several stimuli, we examined whether NTS-induced EGR1 expression is also mediated by MAPK activation in KGN cells. Inhibition of ERK1/2 activation with MEK-1/2 inhibitor U0126 eliminated not only the NTS-induced EGR1 mRNA and protein increase but also the basal expression (Figs. 8I and S8).

SR48692's involvement in mitochondrial dysfunction prompted us to explore the possible impact of EGR1 on mitochondrial function. We found that the ROS generation level in EGR1 knockdown cells was higher than that in the controls, and the ATP concentration was lower (Fig. 8J–8L). These results indicate that EGR1 is a crucial downstream modulator of NTS/NTSR1-induced ERK1/2 phosphorylation, and its depletion impairs cell mitochondrial function.

Discussion

NTS is a gene upregulated in human GCs and mouse ovulatory follicles [48–50] and a potential paracrine regulator of ovulation [51]. NTS and its receptors show abundant expression in the hypothalamus. In the neuroendocrine axis, increased ovarian estradiol secretion

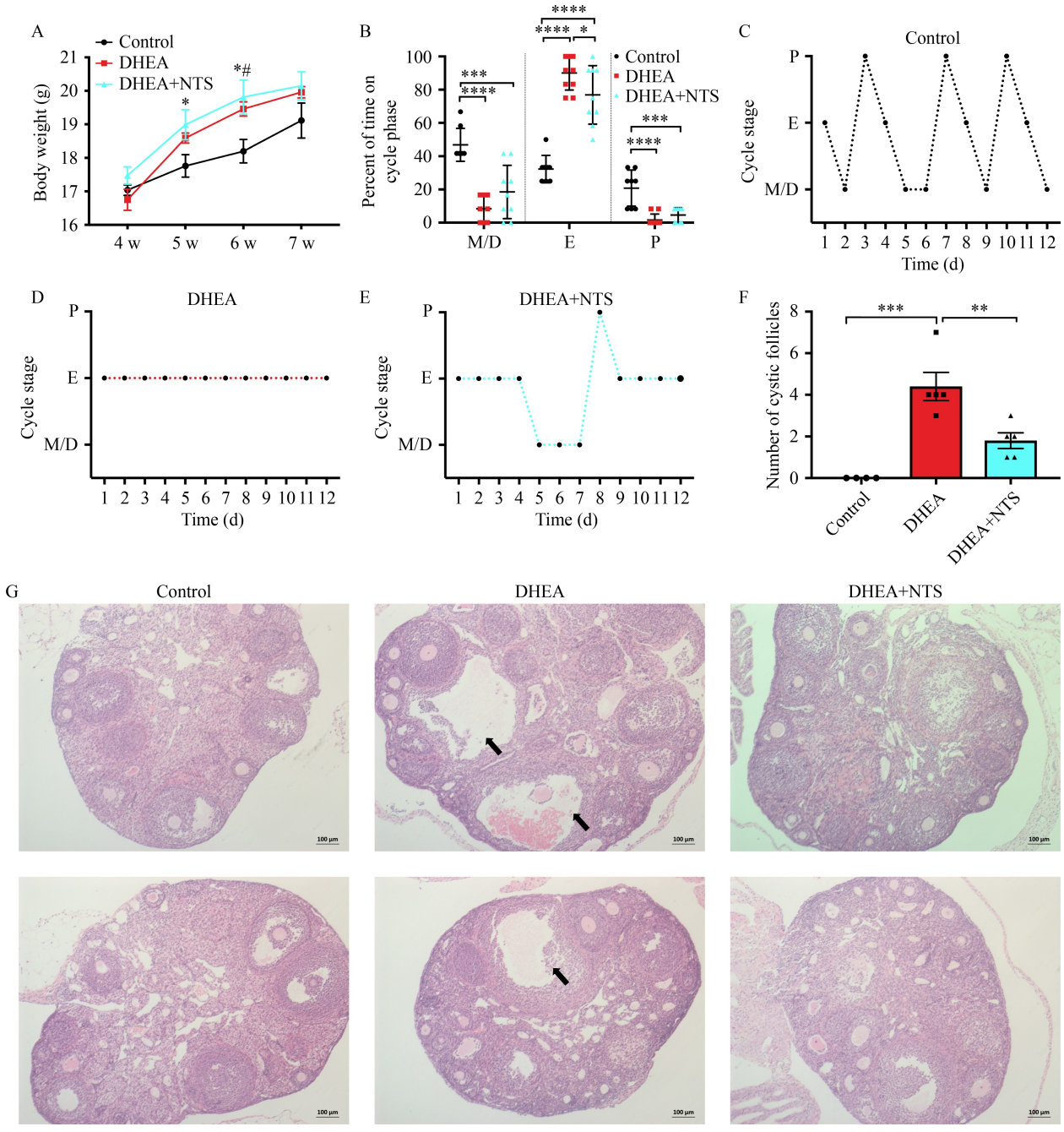

Fig. 7 Neurotensin (NTS) partially improved polycystic ovarian changes in dehydroepiandrosterone (DHEA)-induced PCOS mice. Immature female mice were divided into three groups: control, DHEA (6 mg per 100 g) and DHEA + NTS (1 μg per 15 g) group. (A) Body weight (n = 8–10 per group). (B) Quantitative analysis of ovarian cyclicity. Vaginal cytology was assessed for 12 days. (C–E) Representative estrous cyclicity. (F) Quantitative analysis of cystic follicles (Control: n = 4; DHEA: n = 5; DHEA + NTS: n = 5). (G) Hematoxylin and eosin (H&E) staining of ovaries. Scale bar: 100 μm. Thick arrows indicate the cyst-like appearance of follicles. Data are presented as the mean ± SEM. *P < 0.05 (control vs. DHEA + NTS), #P < 0.05 (control vs. DHEA). *P < 0.05, **P < 0.01, ***P < 0.001, ****P < 0.0001.

activates gonadotropin-releasing hormone (GnRH) neurons in the basal forebrain, which then stimulates the pituitary gland to produce LH and ultimately induce ovulation [52]. Alexander *et al*. [53] found that estradiol increased the number of NTS-immunoreactive cell bodies in the preoptic area of female rats. With the medial preoptic area (MPOA) implicated in the surge of LH, Ferris *et al*. [54] showed that plasma LH levels increased significantly after the microinjection of NTS into the MPOA of ovariectomized rats. After the bilateral microinjections of NTS antiserum at the anterior border of the MPOA, the magnitude of the LH surge decreased without altering its timing, indicating that NTS in the basal forebrain participates in the preovulatory LH surge

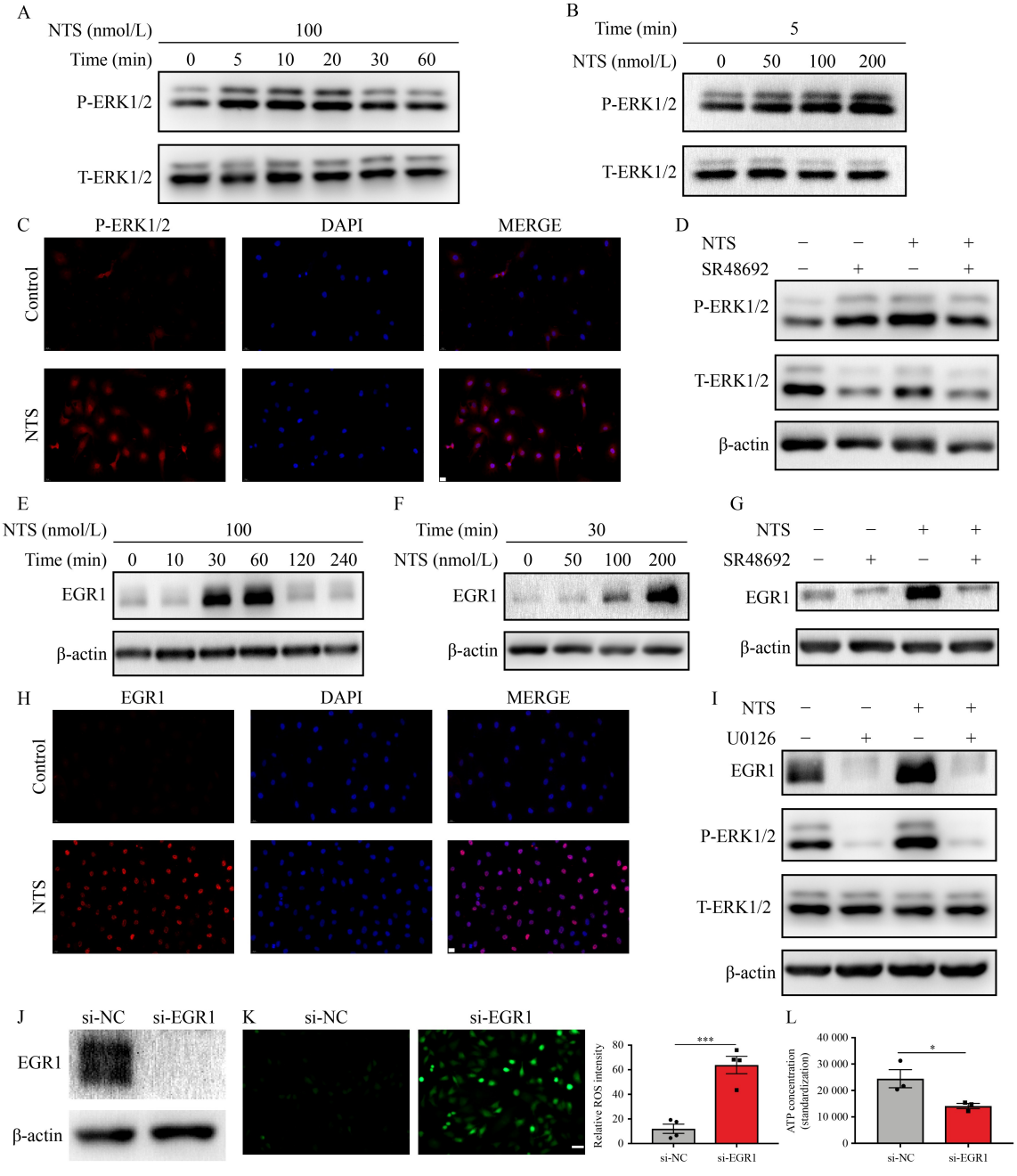

Fig. 8 Neurotensin-induced EGR1 expression was mediated via NTSR1-ERK1/2 in KGN cells. Confluent KGN cells were washed with PBS, incubated in serum-free DMEM/F12 for 6 h, and then treated with 100 nmol/L neurotensin (NTS) for 0 to 60 min (A) or with 0 to 200 nmol/L NTS for 5 min (B). ERK-1/2 phosphorylation was detected in cell lysates by Western blot analysis. The results were standardized to the total levels of ERK-1/2. (C) Nuclear localization of phospho-ERK1/2 in NTS-treated KGN cells (5 min) was examined by immunofluorescent staining. Nuclei were counterstained with DAPI. Scale bar: 20 µm. (D) KGN cells were incubated with DMSO or 10 µmol/L SR48692 in serum-free DMEM/F12 for 6 h and then NTS was added (100 nmol/L, 5 min). Phospho-ERK1/2 was detected in cell lysates by Western blot analysis. (E, F) Confluent KGN cells were washed with PBS, incubated in serum-free DMEM/F12 for 6 h, and then treated with 100 nmol/L NTS for 0 to 4 h or with 0 to 200 nmol/L NTS for 30 min. EGR1 and β-actin protein levels were measured by Western blot analysis (cell lysates). (G) KGN cells were incubated with DMSO or 10 µmol/L SR48692 in serum-free DMEM/F12 for 6 h and then added with NTS (100 nmol/L, 30 min). EGR1 and β-actin protein levels were measured by Western blot analysis (cell lysates). (H) Immunofluorescent staining of NTS-induced nuclear localization of EGR1 protein (red) in KGN cells. Nuclei were counterstained with DAPI. Scale bar: 20 µm. (I) Serum-starved KGN cells were pretreated with DMSO or 10 µmol/L MEK-1/2 inhibitor U0126 for 1 h, followed by 100 nmol/L NTS for 30 min. EGR1 and β-actin protein levels were measured by Western blot analysis (cell lysates). (J) Protein abundance of EGR1 after EGR1 knockdown in KGN cells. (K) Level of intracellular reactive oxygen species (ROS) production was detected by the fluorescence intensity of 2′,7′-dichlorofluorescin diacetate (DCFH-DA) after siRNA-mediated EGR1 knockdown in KGN cells. Scale bar: 50 µm. (L) Concentration of intracellular adenosine triphosphate (ATP) after EGR1 knockdown in KGN cells. Data are shown as the mean ± SEM. *$P < 0.05$, ***$P < 0.001$.

[43]. Conversely, Lemko *et al*. [55] established that NTS does not play a primary role in evoking the GnRH/LH surge in mice. Macaques exhibited unruptured follicles with retained oocytes after the intrafollicular infusion of NTS-neutralizing antibody [14]. These puzzling and contradictory findings on the capability of NTS may arise from variations in methods (e.g., dosage and position of injection) and species. Here, we verified that ovarian NTS transcripts and serum NTS levels reached a maximum 6 h after hCG treatment and returned to baseline 12 h later. Furthermore, the mRNA and protein expression levels of NTS in hCG-induced ovulated COCs were markedly higher than those in immature COCs, illustrating its importance in ovulatory cascades.

NTS biological effects are mediated through multiple membrane receptors: NTSR1 and NTSR2 (high- and low-affinity receptors, respectively) are G protein-coupled receptors, and NTSR3 (sortilin) has a single-transmembrane domain [56]. However, the majority of NTS biological functions are chiefly regulated via NTSR1 [11]. The pharmacological and physiologic features of levocabastine-sensitive NTSR2 are highly debatable because it shows cell-type and species differences. Whether NTS acts as an agonist or antagonist at this site remains unclear. In addition, the effects of sortilin/NTSR3 are poorly understood because this receptor can bind to a wide variety of ligands apart from NTS [57]. Campbell *et al*. [14] established that ovarian follicles express NTS and its receptors during ovulatory processes. However, the role of these receptors in the ovulation cascade requires further in-depth research. PCOS is the most common reason for female anovulatory infertility, but no study describing NTS action in the PCOS pathophysiology has been published.

Our research is the first to illustrate the low NTS expression in the GCs and follicular fluids of females with PCOS. Ovulation includes the coordinated results of sequential processes, such as cumulus expansion, oocyte maturation, follicular rupture, and GC luteinization. The role of NTS in ovulatory cascades was assessed in animal models utilizing the NTSR1-specific antagonist SR48692. Our findings provide the first evidence that SR48692 dose-dependently inhibits cumulus expansion and oocyte meiotic maturation. Furthermore, the possible impacts of SR48692 on cumulus expansion and oocyte maturation were investigated by high-throughput sequencing. Bioinformatics analyses showed the significant enrichment of categories related to metabolic pathways, such as oxidative phosphorylation, glycolysis, and glutathione/amino acid/fatty acid metabolism, suggesting that SR48692 inhibits the metabolic cooperation between oocytes and CCs. Mitochondria are key players in ATP generation by the oxidative phosphorylation system. During the transition from GV to matured oocytes (MII), the distribution of mitochondria markedly changes. We found that SR48692 supplementation impaired the mitochondrial structure, leading to an increase in ROS generation and a steep decline in ATP levels in oocytes and COCs. Consistently, various studies reported that patients with PCOS exhibit mitochondrial dysfunction and oxidative stress [58–61]. Furthermore, we demonstrated that SR48692 treatment markedly decreased ovulation efficiency and induced acyclicity, which were similar to the phenotypes observed with PCOS. These observations suggest that inhibiting NTS action causes ovulatory dysfunction and can be considered a potential inducer of PCOS pathogenesis.

The ERK pathway plays an important role in ovulation [21]. ERK1 and ERK2 are expressed to varying extents in all tissues of mammals and are suggested to be pivotal modulators of oocyte maturation and cumulus expansion under *in vitro* conditions [62]. The obligatory role of ERK1/2 in reproduction was further underscored in genetic studies, which showed that ERK1/2 loss in ovarian GCs or in the anterior pituitary causes female infertility and failure in ovulation [21,63]. In addition, EKR1/2 signaling controls EGR1 expression [64], an important transcription factor involved in regulating cell proliferation, differentiation, angiogenesis, ovulation, and fertility [25,65]. EGR1 is sited in the granulosa and theca interna layers of the larger antral follicles, corpora lutea, and pituitary [66]. Previous studies illustrated that the impact of NTS/NTSR1 stimulation on cell growth and DNA synthesis is mainly mediated by the MEK/ERK1/2 phosphorylation pathway in several cancers [30]. However, whether this pathway participates in ovulation remains unclear. Here, we identified EGR1 as the candidate target of NTS/NTSR1 based on RNA-seq analyses, and its expression was ovulation-dependent. In addition, *Egr1* depletion in GV oocytes by siRNA led to impaired oocyte maturation.

To further explore the ovulation-blocking impacts of SR48692 at the molecular level, we examined the expression of related markers in ovaries from different mouse models and verified the signaling pathway in KGN cells. Treatment with the NTSR1 antagonist SR48692 profoundly inhibited ERK1/2 phosphorylation and EGR1 expression *in vivo* and *in vitro*. EGR1 depletion significantly increased ROS deposition and decreased ATP generation. Recent studies also demonstrated that EGR1 mediates metabolic reprogramming to oxidative phosphorylation. In particular, EGR1 knockdown significantly reduces mitochondrial membrane potential and ATP production [67]. High amounts of ERK are present in the mitochondria. Blocking ERK activity causes a rapid and severe decrease in cellular ATP and disrupts mitochondrial transmembrane potential [68]. Overall, these results indicate that the NTS-NTSR1 interaction takes part in the ovulatory process mediated by the ERK/EGR1 signaling pathway.

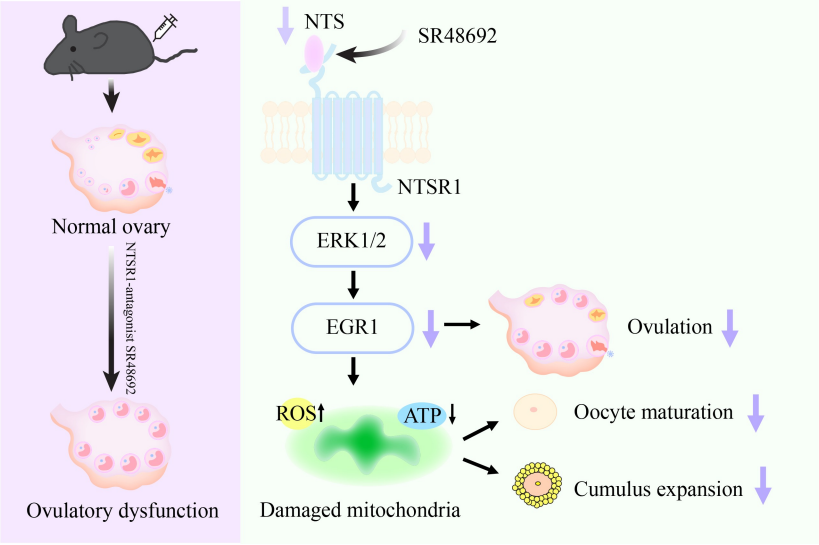

Fig. 9 Schematic of decreased neurotensin contributing to ovulatory dysfunction via the NTSR1/ERK/EGR1 axis.

The subfertility of variable severity in PCOS is due to infrequent or absent ovulation. Furthermore, a subgroup of women with PCOS exhibit polycystic ovarian morphology, identified by increased thecal-stromal volume and elevated numbers of follicles surrounding the ovarian cortex. In view of the growing evidence for the role of NTS in ovulation, we further investigated whether NTS treatment might ameliorate ovarian abnormalities in mice with PCOS. We found that NTS administration partially improved DHEA-induced estrous acyclicity and decreased the number of fluid-filled cystic follicles and small antral follicles in PCOS-like mice. However, NTS treatment could not alleviate weight gain, suggesting that PCOS is a complicated syndrome involving multiple factors and monotherapy may not be sufficient to treat all its symptoms.

Adult *Nts*$^{-/-}$ mice resemble wild-type mice in reproduction [69,70]; however, this issue has not yet been extensively studied, and whether *Nts*$^{-/-}$ female mice are completely fertile remains unclear. Knocking out a gene at times has no discernible effect in mice, and antisense reagents that block the same targets lead to profound defects [71]. These differences have been attributed to many reasons, including off-target or toxic impacts of the chemical agents and mutation-induced biological compensation [72]. Thus, a tissue-specific NTS conditional loss-of-function might avoid the disadvantages caused by global knockout models, and the phenotype might be accurately linked to deactivation of the target gene in some way [73].

One of the limitations of our study is that we focused solely on NTSR1 as an important high-affinity receptor of NTS for the modulation of ovulatory dysfunction in PCOS due to time and technical constraints. Other receptors of NTS may participate in the regulation of reproductive functions. For instance, NTSR3 is highly expressed in follicular theca, granulosa, and endothelial cells, and its level can be elevated by PGE2, an important paracrine factor of ovulation [14]. Further detailed studies will be required to assess the effect of NTS receptors on ovulatory cascades. Second, although nonluteinized human GCs are the best cell model, we could not obtain them due to current technical restrictions. Hence, we utilized KGN cells, a human granulosa-like tumor cell line, for *in vitro* experiments. Further work will be needed to verify our observations in primate models and, to the extent possible, in clinical trials. Efficient NTS depletion in mutant GCs and oocytes in mouse models is required to further explore the definite effects of NTS on reproductive function.

In summary, we illustrated the role of NTS/NTSR1 in the development of ovulatory dysfunction in PCOS. The profound impacts of aberrant NTS on NTSR1/ERK/EGR1 pathways and mitochondria dysfunction may cause the blockade of ovulation, including cumulus expansion, oocyte maturation, and follicular rupture (Fig. 9). NTS administration may provide a potential opportunity for the pharmacological alleviation of anovulation in PCOS. Further studies are required to verify our hypothesis. A comprehensive understanding of the exact mechanisms of NTS during ovulation may contribute to the therapy for certain kinds of infertility.

Acknowledgements

This work was supported by grants from the National Key Research and Development Program of China (Nos. 2022YFC2703204 and 2021YFC2701104), the National Natural Science Foundation of China (Nos. 81971343 and 82171623), the National Institutes of Health Project (No. 1R01HD085527), the

Innovative research team of high-level local universities in Shanghai (No. SHSMU-ZLCX20210200), Shanghai Commission of Science and Technology (Nos. 21XD1401900 and 20DZ2270900), Three-Year Action Plan for Strengthening the Construction of the Public Health System in Shanghai (No. GWVI-11.1-36) and Shanghai's Top Priority Research Center Construction Project (No. 2023ZZ02002).

Compliance with ethics guidelines

Conflicts of interest Dongshuang Wang, Meiling Zhang, Wang-Sheng Wang, Weiwei Chu, Junyu Zhai, Yun Sun, Zi-Jiang Chen and Yanzhi Du declare that they have no competing interests.

The study was approved by the Ethics Committee of Ren Ji hospital, Shanghai Jiao Tong University School of Medicine and the study was performed in accordance with the ethical standards as laid down in the 1964 *Declaration of Helsinki* and its later amendments or comparable ethical standards. Informed consent was obtained from all patients for being included in the study. All institutional and national guidelines for the care and use of laboratory animals were followed.

Electronic Supplementary Material Supplementary material is available in the online version of this article at https://doi.org/10.1007/s11684-024-1089-z and is accessible for authorized users.

References

1. Azziz R, Carmina E, Chen Z, Dunaif A, Laven JSE, Legro RS, Lizneva D, Natterson-Horowtiz B, Teede HJ, Yildiz BO. Polycystic ovary syndrome. Nat Rev Dis Primers 2016; 2(1): 16057
2. Carson SA, Kallen AN. Diagnosis and management of infertility: a review. JAMA 2021; 326(1): 65–76
3. Qiao J, Feng HL. Extra- and intra-ovarian factors in polycystic ovary syndrome: impact on oocyte maturation and embryo developmental competence. Hum Reprod Update 2011; 17(1): 17–33
4. Liu Q, Li Y, Feng Y, Liu C, Ma J, Li Y, Xiang H, Ji Y, Cao Y, Tong X, Xue Z. Single-cell analysis of differences in transcriptomic profiles of oocytes and cumulus cells at GV, MI, MII stages from PCOS patients. Sci Rep 2016; 6(1): 39638
5. Lénárd L, László K, Kertes E, Ollmann T, Péczely L, Kovács A, Kállai V, Zagorácz O, Gálosi R, Karádi Z. Substance P and neurotensin in the limbic system: their roles in reinforcement and memory consolidation. Neurosci Biobehav Rev 2018; 85: 1–20
6. Tabarean IV. Neurotensin induces hypothermia by activating both neuronal neurotensin receptor 1 and astrocytic neurotensin receptor 2 in the median preoptic nucleus. Neuropharmacology 2020; 171: 108069
7. Kurt G, Woodworth HL, Fowler S, Bugescu R, Leinninger GM. Activation of lateral hypothalamic area neurotensin-expressing neurons promotes drinking. Neuropharmacology 2019; 154: 13–21
8. Richner M, Pallesen LT, Ulrichsen M, Poulsen ET, Holm TH, Login H, Castonguay A, Lorenzo LE, Gonçalves NP, Andersen OM, Lykke-Hartmann K, Enghild JJ, Rønn LCB, Malik IJ, De Koninck Y, Bjerrum OJ, Vægter CB, Nykjær A. Sortilin gates neurotensin and BDNF signaling to control peripheral neuropathic pain. Sci Adv 2019; 5(6): eaav9946
9. Ma C, Zhong P, Liu D, Barger ZK, Zhou L, Chang WC, Kim B, Dan Y. Sleep regulation by neurotensinergic neurons in a thalamo-amygdala circuit. Neuron 2019; 103(2): 323–334.e7
10. Deluigi M, Klipp A, Klenk C, Merklinger L, Eberle SA, Morstein L, Heine P, Mittl PRE, Ernst P, Kamenecka TM, He Y, Vacca S, Egloff P, Honegger A, Plückthun A. Complexes of the neurotensin receptor 1 with small-molecule ligands reveal structural determinants of full, partial, and inverse agonism. Sci Adv 2021; 7(5): eabe5504
11. Christou N, Blondy S, David V, Verdier M, Lalloué F, Jauberteau MO, Mathonnet M, Perraud A. Neurotensin pathway in digestive cancers and clinical applications: an overview. Cell Death Dis 2020; 11(12): 1027
12. Liu J, Agopiantz M, Poupon J, Wu Z, Just PA, Borghese B, Ségal-Bendirdjian E, Gauchotte G, Gompel A, Forgez P. Neurotensin receptor 1 antagonist SR48692 improves response to carboplatin by enhancing apoptosis and inhibiting drug efflux in ovarian cancer. Clin Cancer Res 2017; 23(21): 6516–6528
13. Norris EJ, Zhang Q, Jones WD, DeStephanis D, Sutker AP, Livasy CA, Ganapathi RN, Tait DL, Ganapathi MK. Increased expression of neurotensin in high grade serous ovarian carcinoma with evidence of serous tubal intraepithelial carcinoma. J Pathol 2019; 248(3): 352–362
14. Campbell GE, Bender HR, Parker GA, Curry TE Jr, Duffy DM. Neurotensin: a novel mediator of ovulation? FASEB J 2021; 35(4): e21481
15. Richards JS, Ascoli M. Endocrine, paracrine, and autocrine signaling pathways that regulate ovulation. Trends Endocrinol Metab 2018; 29(5): 313–325
16. Eppig JJ, Pendola FL, Wigglesworth K, Pendola JK. Mouse oocytes regulate metabolic cooperativity between granulosa cells and oocytes: amino acid transport. Biol Reprod 2005; 73(2): 351–357
17. Su YQ, Sugiura K, Eppig JJ. Mouse oocyte control of granulosa cell development and function: paracrine regulation of cumulus cell metabolism. Semin Reprod Med 2009; 27(1): 32–42
18. Martinez CA, Rizos D, Rodriguez-Martinez H, Funahashi H. Oocyte-cumulus cells crosstalk: new comparative insights. Theriogenology 2023; 205: 87–93
19. Seli E, Wang T, Horvath TL. Mitochondrial unfolded protein response: a stress response with implications for fertility and reproductive aging. Fertil Steril 2019; 111(2): 197–204
20. van der Reest J, Nardini Cecchino G, Haigis MC, Kordowitzki P. Mitochondria: their relevance during oocyte ageing. Ageing Res Rev 2021; 70: 101378
21. Fan HY, Liu Z, Shimada M, Sterneck E, Johnson PF, Hedrick SM, Richards JS. MAPK3/1 (ERK1/2) in ovarian granulosa cells are essential for female fertility. Science 2009; 324(5929): 938–941
22. Bongartz H, Seiß EA, Bock J, Schaper F. Glucocorticoids attenuate interleukin-6-induced c-Fos and Egr1 expression and impair neuritogenesis in PC12 cells. J Neurochem 2021; 157(3): 532–549
23. Cook PJ, Thomas R, Kingsley PJ, Shimizu F, Montrose DC, Marnett LJ, Tabar VS, Dannenberg AJ, Benezra R. Cox-2-derived PGE2 induces Id1-dependent radiation resistance and self-renewal

in experimental glioblastoma. Neuro-oncol 2016; 18(10): 1379–1389
24. Carletti MZ, Christenson LK. Rapid effects of LH on gene expression in the mural granulosa cells of mouse periovulatory follicles. Reproduction 2009; 137(5): 843–855
25. Topilko P, Schneider-Maunoury S, Levi G, Trembleau A, Gourdji D, Driancourt MA, Rao CV, Charnay P. Multiple pituitary and ovarian defects in Krox-24 (NGFI-A, Egr-1)-targeted mice. Mol Endocrinol 1998; 12(1): 107–122
26. Iyoda T, Zhang F, Sun L, Hao F, Schmitz-Peiffer C, Xu X, Cui MZ. Lysophosphatidic acid induces early growth response-1 (Egr-1) protein expression via protein kinase Cδ-regulated extracellular signal-regulated kinase (ERK) and c-Jun N-terminal kinase (JNK) activation in vascular smooth muscle cells. J Biol Chem 2012; 287(27): 22635–22642
27. Khachigian LM. The MEK-ERK-Egr-1 axis and its regulation in cardiovascular disease. Vascul Pharmacol 2023; 153: 107232
28. Rotterdam ESHRE/ASRM-Sponsored PCOS Consensus Workshop Group. Revised 2003 consensus on diagnostic criteria and long-term health risks related to polycystic ovary syndrome. Fertil Steril 2004; 81(1): 19–25
29. Zhou R, Li S, Liu J, Wu H, Yao G, Sun Y, Chen ZJ, Li W, Du Y. Up-regulated FHL2 inhibits ovulation through interacting with androgen receptor and ERK1/2 in polycystic ovary syndrome. EBioMedicine 2020; 52: 102635
30. Ouyang Q, Gong X, Xiao H, Zhou J, Xu M, Dai Y, Xu L, Feng H, Cui H, Yi L. Neurotensin promotes the progression of malignant glioma through NTSR1 and impacts the prognosis of glioma patients. Mol Cancer 2015; 14(1): 21
31. Qi X, Zhang B, Zhao Y, Li R, Chang HM, Pang Y, Qiao J. Hyperhomocysteinemia promotes insulin resistance and adipose tissue inflammation in PCOS mice through modulating M2 macrophage polarization via estrogen suppression. Endocrinology 2017; 158(5): 1181–1193
32. Shen H, Xu X, Fu Z, Xu C, Wang Y. The interactions of CAP and LYN with the insulin signaling transducer CBL play an important role in polycystic ovary syndrome. Metabolism 2022; 131: 155164
33. Myers M, Britt KL, Wreford NGM, Ebling FJP, Kerr JB. Methods for quantifying follicular numbers within the mouse ovary. Reproduction 2004; 127(5): 569–580
34. Tata B, Mimouni NEH, Barbotin AL, Malone SA, Loyens A, Pigny P, Dewailly D, Catteau-Jonard S, Sundström-Poromaa I, Piltonen TT, Dal Bello F, Medana C, Prevot V, Clasadonte J, Giacobini P. Elevated prenatal anti-Müllerian hormone reprograms the fetus and induces polycystic ovary syndrome in adulthood. Nat Med 2018; 24(6): 834–846
35. Caldwell ASL, Middleton LJ, Jimenez M, Desai R, McMahon AC, Allan CM, Handelsman DJ, Walters KA. Characterization of reproductive, metabolic, and endocrine features of polycystic ovary syndrome in female hyperandrogenic mouse models. Endocrinology 2014; 155(8): 3146–3159
36. Han D, Zhao BT, Liu Y, Li JJ, Wu YG, Lan GC, Tan JH. Interactive effects of low temperature and roscovitine (ROS) on meiotic resumption and developmental potential of goat oocytes. Mol Reprod Dev 2008; 75(5): 838–846
37. Vanderhyden BC, Caron PJ, Buccione R, Eppig JJ. Developmental pattern of the secretion of cumulus expansion-enabling factor by mouse oocytes and the role of oocytes in promoting granulosa cell differentiation. Dev Biol 1990; 140(2): 307–317
38. Fagbohun CF, Downs SM. Maturation of the mouse oocyte-cumulus cell complex: stimulation by lectins. Biol Reprod 1990; 42(3): 413–423
39. Marangos P, Verschuren EW, Chen R, Jackson PK, Carroll J. Prophase I arrest and progression to metaphase I in mouse oocytes are controlled by Emi1-dependent regulation of APC(Cdh1). J Cell Biol 2007; 176(1): 65–75
40. Picelli S, Faridani OR, Björklund AK, Winberg G, Sagasser S, Sandberg R. Full-length RNA-seq from single cells using Smart-seq2. Nat Protoc 2014; 9(1): 171–181
41. Li J, Song J, Zaytseva YY, Liu Y, Rychahou P, Jiang K, Starr ME, Kim JT, Harris JW, Yiannikouris FB, Katz WS, Nilsson PM, Orho-Melander M, Chen J, Zhu H, Fahrenholz T, Higashi RM, Gao T, Morris AJ, Cassis LA, Fan TWM, Weiss HL, Dobner PR, Melander O, Jia J, Evers BM. An obligatory role for neurotensin in high-fat-diet-induced obesity. Nature 2016; 533(7603): 411–415
42. Brethvad AO, Zakariassen HL, Holt J, Lundgren JR, Jakobsen A, Hartmann B, Lehmann EW, Kissow H, Holst JJ, Madsbad S, Torekov SS, Holst B. Increased meal-induced neurotensin response predicts successful maintenance of weight loss—Data from a randomized controlled trial. Metabolism 2023; 143: 155534
43. Alexander MJ, Mahoney PD, Ferris CF, Carraway RE, Leeman SE. Evidence that neurotensin participates in the central regulation of the preovulatory surge of luteinizing hormone in the rat. Endocrinology 1989; 124(2): 783–788
44. Wang Q, Sun QY. Evaluation of oocyte quality: morphological, cellular and molecular predictors. Reprod Fertil Dev 2007; 19(1): 1
45. Richani D, Dunning KR, Thompson JG, Gilchrist RB. Metabolic co-dependence of the oocyte and cumulus cells: essential role in determining oocyte developmental competence. Hum Reprod Update 2021; 27(1): 27–47
46. Fontana J, Martínková S, Petr J, Žalmanová T, Trnka J. Metabolic cooperation in the ovarian follicle. Physiol Res 2020; 69(1): 33–48
47. Kirillova A, Smitz JEJ, Sukhikh GT, Mazunin I. The role of mitochondria in oocyte maturation. Cells 2021; 10(9): 2484
48. Al-Alem L, Puttabyatappa M, Shrestha K, Choi Y, Rosewell K, Brännström M, Akin J, Jo M, Duffy DM, Curry TE Jr. Neurotensin: a neuropeptide induced by hCG in the human and rat ovary during the periovulatory period. Biol Reprod 2021; 104(6): 1337–1346
49. Hiradate Y, Inoue H, Kobayashi N, Shirakata Y, Suzuki Y, Gotoh A, Roh SG, Uchida T, Katoh K, Yoshida M, Sato E, Tanemura K. Neurotensin enhances sperm capacitation and acrosome reaction in mice. Biol Reprod 2014; 91(2): 53
50. Shrestha K, Al-Alem L, Garcia P, Wynn MAA, Hannon PR, Jo M, Drnevich J, Duffy DM, Curry TE Jr. Neurotensin expression, regulation, and function during the ovulatory period in the mouse ovary. Biol Reprod 2023; 108(1): 107–120
51. Arbogast P, Gauchotte G, Mougel R, Morel O, Ziyyat A, Agopiantz M. Neurotensin and its involvement in reproductive functions: an exhaustive review of the literature. Int J Mol Sci 2023; 24(5): 4594
52. Kim J, Bagchi IC, Bagchi MK. Control of ovulation in mice by progesterone receptor-regulated gene networks. Mol Hum Reprod 2009; 15(12): 821–828
53. Alexander MJ, Leeman SE. Estrogen-inducible neurotensin immunoreactivity in the preoptic area of the female rat. J Comp

Neurol 1994; 345(4): 496–509
54. Ferris CF, Pan JX, Singer EA, Boyd ND, Carraway RE, Leeman SE. Stimulation of luteinizing hormone release after stereotaxic microinjection of neurotensin into the medial preoptic area of rats. Neuroendocrinology 1984; 38(2): 145–151
55. Dungan Lemko HM, Naderi R, Adjan V, Jennes LH, Navarro VM, Clifton DK, Steiner RA. Interactions between neurotensin and GnRH neurons in the positive feedback control of GnRH/LH secretion in the mouse. Am J Physiol Endocrinol Metab 2010; 298(1): E80–E88
56. Alexander SPH, Christopoulos A, Davenport AP, Kelly E, Mathie A, Peters JA, Veale EL, Armstrong JF, Faccenda E, Harding SD, Pawson AJ, Sharman JL, Southan C, Davies JA. The concise guide to pharmacology 2019/20: G protein-coupled receptors. Br J Pharmacol 2019; 176 (S1 Suppl 1)
57. Mazella J, Vincent JP. Functional roles of the NTS2 and NTS3 receptors. Peptides 2006; 27(10): 2469–2475
58. Dabravolski SA, Nikiforov NG, Eid AH, Nedosugova LV, Starodubova AV, Popkova TV, Bezsonov EE, Orekhov AN. Mitochondrial dysfunction and chronic inflammation in polycystic ovary syndrome. Int J Mol Sci 2021; 22(8): 3923
59. Kaltsas A, Zikopoulos A, Moustakli E, Zachariou A, Tsirka G, Tsiampali C, Palapela N, Sofikitis N, Dimitriadis F. The silent threat to women's fertility: uncovering the devastating effects of oxidative stress. Antioxidants 2023; 12(8): 1490
60. Zeber-Lubecka N, Ciebiera M, Hennig EE. Polycystic ovary syndrome and oxidative stress-from bench to bedside. Int J Mol Sci 2023; 24(18): 14126
61. Zhang Q, Ren J, Wang F, Pan M, Cui L, Li M, Qu F. Mitochondrial and glucose metabolic dysfunctions in granulosa cells induce impaired oocytes of polycystic ovary syndrome through Sirtuin 3. Free Radic Biol Med 2022; 187: 1–16
62. Su YQ, Wigglesworth K, Pendola FL, O'Brien MJ, Eppig JJ. Mitogen-activated protein kinase activity in cumulus cells is essential for gonadotropin-induced oocyte meiotic resumption and cumulus expansion in the mouse. Endocrinology 2002; 143(6): 2221–2232
63. Bliss SP, Miller A, Navratil AM, Xie J, McDonough SP, Fisher PJ, Landreth GE, Roberson MS. ERK signaling in the pituitary is required for female but not male fertility. Mol Endocrinol 2009; 23(7): 1092–1101
64. Guha M, O'Connell MA, Pawlinski R, Hollis A, McGovern P, Yan SF, Stern D, Mackman N. Lipopolysaccharide activation of the MEK-ERK1/2 pathway in human monocytic cells mediates tissue factor and tumor necrosis factor alpha expression by inducing Elk-1 phosphorylation and Egr-1 expression. Blood 2001; 98(5): 1429–1439
65. Guo B, Tian XC, Li DD, Yang ZQ, Cao H, Zhang QL, Liu JX, Yue ZP. Expression, regulation and function of Egr1 during implantation and decidualization in mice. Cell Cycle 2014; 13(16): 2626–2640
66. Schuermann Y, Rovani MT, Gasperin B, Ferreira R, Ferst J, Madogwe E, Gonçalves PB, Bordignon V, Duggavathi R. ERK1/2-dependent gene expression in the bovine ovulating follicle. Sci Rep 2018; 8(1): 16170
67. Liu Y, Kimpara S, Hoang NM, Daenthanasanmak A, Li Y, Lu L, Ngo VN, Bates PD, Song L, Gao X, Bebel S, Chen M, Chen R, Zhang X, Selberg PE, Kenkre VP, Waldmann TA, Capitini CM, Rui L. EGR1-mediated metabolic reprogramming to oxidative phosphorylation contributes to ibrutinib resistance in B-cell lymphoma. Blood 2023; 142(22): 1879–1894
68. Monick MM, Powers LS, Barrett CW, Hinde S, Ashare A, Groskreutz DJ, Nyunoya T, Coleman M, Spitz DR, Hunninghake GW. Constitutive ERK MAPK activity regulates macrophage ATP production and mitochondrial integrity. J Immunol 2008; 180(11): 7485–7496
69. Dobner PR, Fadel J, Deitemeyer N, Carraway RE, Deutch AY. Neurotensin-deficient mice show altered responses to antipsychotic drugs. Proc Natl Acad Sci USA 2001; 98(14): 8048–8053
70. Piliponsky AM, Chen CC, Nishimura T, Metz M, Rios EJ, Dobner PR, Wada E, Wada K, Zacharias S, Mohanasundaram UM, Faix JD, Abrink M, Pejler G, Pearl RG, Tsai M, Galli SJ. Neurotensin increases mortality and mast cells reduce neurotensin levels in a mouse model of sepsis. Nat Med 2008; 14(4): 392–398
71. El-Brolosy MA, Stainier DYR. Genetic compensation: a phenomenon in search of mechanisms. PLoS Genet 2017; 13(7): e1006780
72. Wilkinson MF. Genetic paradox explained by nonsense. Nature 2019; 568(7751): 179–180
73. Yerushalmi GM, Markman S, Yung Y, Maman E, Aviel-Ronen S, Orvieto R, Adashi EY, Hourvitz A. The prostaglandin transporter (PGT) as a potential mediator of ovulation. Sci Transl Med 2016; 8(338): 338ra368